國立臺灣大學工學院土木工程學系

碩士論文

Graduate Institute of Civil Engineering
College of Engineering
National Taiwan University

Master Thesis

深開挖基地三維幾何配置於連續壁壁體變位之影響

The Effect of Three Dimensional Configurations on the Diaphragm Wall Displacements Due to Deep Excavation

張智博

Chih-Po Chang

指導教授：葛宇甯 教授

Advisor: Prof. Louis Ge

中華民國 105 年 6 月

June, 2016

doi:10.6342/NTU201600809

doi:10.6342/NTU201600809

誌謝

兩年。

回首這些日子，見到自己緩慢但穩健地走了一段路，甚感欣慰。

感謝指導老師 葛宇甯教授，在我和此研究上挹注了許多資源以及心力，並給予足夠的空間選擇研究的方法且不厭其煩地讓我嘗試與修正，使我碩士生涯十分充實。

感謝同窗黃郁惟在報告前總耐心地聽我練習並給予意見，甚至一起討論研究的方法以及盲點。

感謝同窗王棋立提供 BIC 以及 SVM 的應用技術，使我能夠更廣泛地嘗試各種方法進行研究。

感謝女友蕭至妤這幾年來的包容，包容我經常地晚歸，以及常常以作研究為藉口，躲在研究室不回家做家事。

最感謝父母，在我就學期間提供精神以及經濟上的支持，讓我能夠心無旁騖地埋首於課業及研究中。

最後，還記得國中時的各種荒唐行徑，感謝 秦冀萍老師及時拉住我，否則我甚至會選擇不繼續升學。

台大魔甘娜之王，畢業啦!

doi:10.6342/NTU201600809

doi:10.6342/NTU201600809

ABSTRACT

Diaphragm walls are often used to resist lateral earth pressure and prevent excess ground settlement and wall movements during excavations. There are several practical methods for diaphragm wall design, based on the assumption of plane strain condition. This assumption is valid for shallow and wide excavations, with L/He value greater than 6 (L: length of diaphragm wall, He: depth of excavation). Due to limited available space in urban area, lots of excavations are small but deep in Taiwan. Without considering the three dimensional effects, it leads to an over conservative design for the diaphragm wall.

To develop an economical method for diaphragm wall design with consideration of three dimensional effect, the finite element software “Plaxis” was used to examine the maximum wall deflection in various combinations of thickness of wall, average vertical and horizontal spacing of struts, length and width of excavation, and maximum ground water head difference.

From the simulation results, the new system stiffness was proposed. As the current study focuses on the excavations in sand, case histories excavated mainly in the sandy layer were selected to verify the applicability of the proposed system stiffness. It was concluded that the proposed system stiffness can quantify the wall stiffness more precisely with consideration of the three dimensional effects, especially in the condition of high system stiffness.

doi:10.6342/NTU201600809

摘要

連續壁常見於深開挖工程之擋土系統，用以抵抗側向土壓力並防止開挖工址周圍產生過大的地表沉陷量造成損鄰。目前實務中，連續壁設計方法多建立於平面應變條件之上；然而此條件適於較淺且較廣的開挖工程，即開挖長度(L)與開挖深度(H_e)比值高於 6 者。因空間有限，臺灣現今於市區及近郊的深開挖工程多呈小且深之設計，已不符平面應變條件之假設；倘若不思三向度效應，將導致擋土系統過度設計，所耗成本甚鉅。

為發展考量三向度效應之連續壁設計方法，此研究採用有限元素分析軟體 Plaxis 模擬於砂土中開挖引致的連續壁壁體變形行為，分析三向度幾何因子，如壁體厚度、平均垂直與水平支撐間距、開挖基地之長與寬等，以及外力因子，基地內外最大水頭差，對於連續壁壁體最大變形量所造成的影響。

根據上述之模擬結果，歸納出可考量三向度效應的新系統勁度。因本研究著眼於砂土中開挖的連續壁壁體變形行為，故採用地層主要由砂性土壤組成之案例驗證所提出之系統勁度。

本研究提出之系統勁度於高勁度擋土系統之預測較為準確。

doi:10.6342/NTU201600809

doi:10.6342/NTU201600809

CONTENTS

doi:10.6342/NTU201600809

doi:10.6342/NTU201600809

LIST OF FIGURES

doi:10.6342/NTU201600809

doi:10.6342/NTU201600809

LIST OF TABLES

doi:10.6342/NTU201600809

doi:10.6342/NTU201600809

Chapter 1 Introduction

Diaphragm walls are usually used as a part of the retaining system during foundation excavation. Current design specifications in Taiwan are primarily focused on the stabilities of the retaining system, which are based on the force or moment equilibrium at the ultimate state. In a modern city, newly constructed structures and facilities are often adjacent to existing structures, such as neighboring buildings, MRT tunnels and so on. In order to minimize the damage to the neighboring structures, the wall-deformation-controlled deign method is in place, where the finite element method (FEM) is a powerful way to simulate the behavior of the retaining system.

Most FEM simulations are conducted by two dimensional models, with an assumption of plane strain for the excavation. This leads to an overestimation of the diaphragm wall deformations. Thus, it is necessary to examine the three dimensional effect in excavations.

1.1 Motivation

The excavations have become deeper and narrower in Taiwan, especially in Taipei city, for decades. For those small and deep excavations, three dimensional effect plays an important role to wall deformation. However, two dimensional finite element method is usually used in practice because it is inexpensive in modeling and calculation. Therefore, a new system stiffness involving three dimensional effect is needed.

1.2 Research Methodology

Two case histories of excavations with different construction methods were studied to examine the modeling method.

Next, 8 geometric configuration factors of excavation were chosen as variables to

doi:10.6342/NTU201600809

model 4860 three dimensional finite element models for simulating wall deformations for top-down excavations.

Then, 9720 sets of wall deformations (each side of excavation can be considered as 1 set of geometric configuration because the L and B could be interchanged, see details in chapter 4.) were used for regression analyses to propose a new system stiffness for the excavation.

Finally, one of the case histories, which was constructed by top-down method, was used to examine the proposed system stiffness and prediction of the regression formula. The research methodology can be seen more briefly in Fig.1.1.

1.3 Thesis Outline

There are 5 chapters in this thesis. The introduction, including motivation and research methodology, is given in the chapter 1. Previous work on the three dimensional effect, plane strain ratio and relative system stiffness are reviewed and summarized in chapter 2. In the chapter 3, two case histories are studied and simulated. Chapter 4 discusses the settings of three dimensional finite element models and the results of simulations. The conclusions and recommendations to future work are described in the chapter 5.

doi:10.6342/NTU201600809

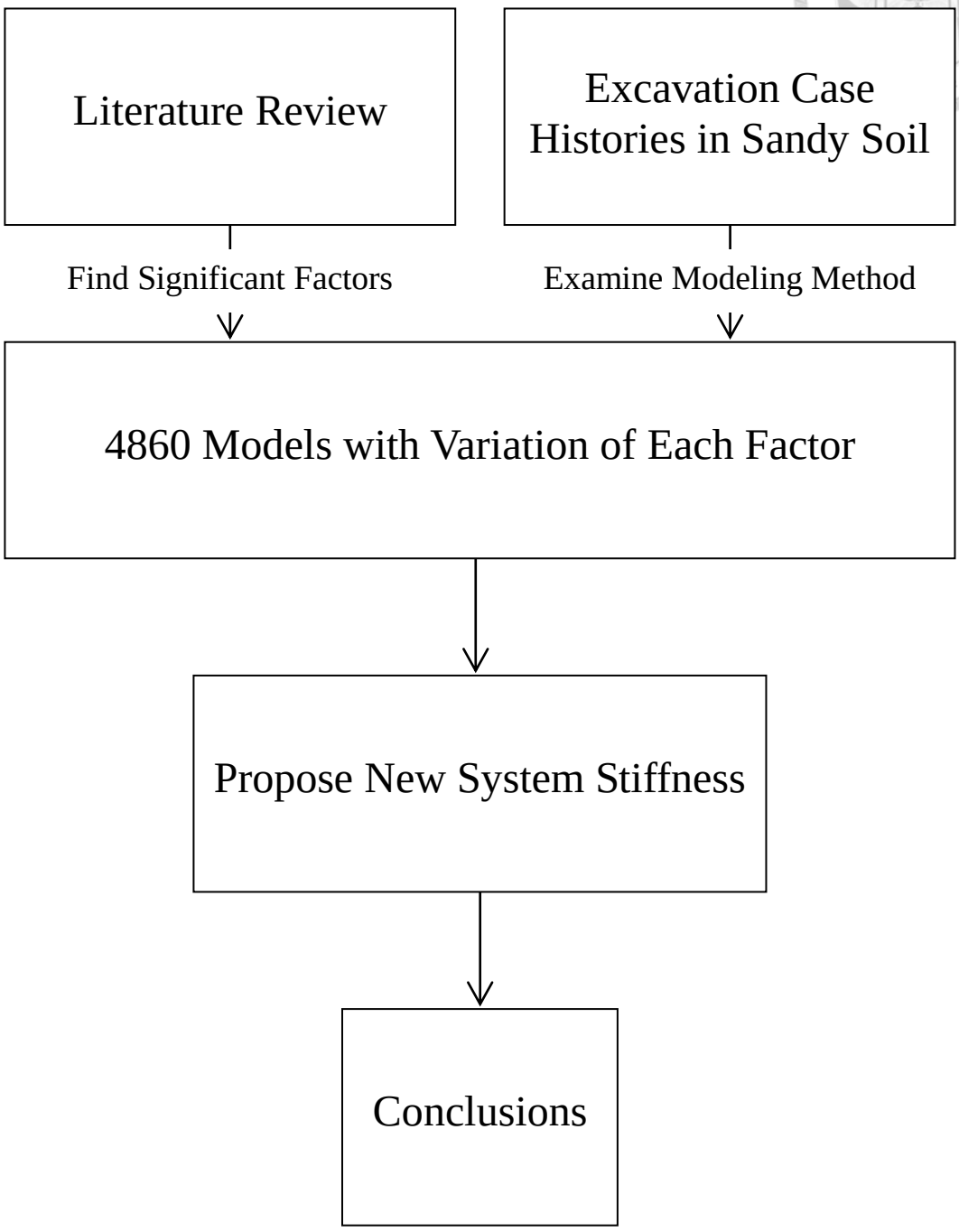

Fig. 1 1 Flow chart of research methodology

doi:10.6342/NTU201600809

Chapter 2 Literature Review

Clough et al. (1989) proposed a chart (Fig. 2.1) for engineers to design the retaining system for excavations. However, this chart is more suitable for soldier piles, sheet piles and the likes, whose wall stiffness is flexible and the excavation depth is shallow, than deep excavations today. Dimension of Excavations becomes smaller but deeper nowadays in Taiwan. The retaining wall system becomes stiffer, where the three dimensional effect would affect the deformation of the diaphragm walls significantly. Therefore, this chart, or other theories under plane strain assumption, would lead to very conservative designs.

The three dimensional effect could be roughly divided into two mechanisms, the soil arching effect and the corner effect. The definition of soil arching was presented by Terzaghi (1943). It can be applied to excavations. When the diaphragm walls and the adjacent soil mass move against each other, the movement would be resisted by shear stresses. The pressure of the moving soil mass is reduced while the pressure of adjacent rigid soil mass is increased (Fig. 2.2). The soil arching effect can be subdivided into active and passive archings, depending upon the direction of the relative movements, as shown in Fig. 2.3.

Three dimensional effects in deep excavation are contributed by several factors, including excavation depth, height of diaphragm wall, length and width of excavation, horizontal and vertical spacing of struts, and so on. There are mainly two approaches to account for the three dimensional effects, plane strain ratio (PSR) and relative stiffness ratio. They are described in this chapter.

doi:10.6342/NTU201600809

2.1 Plane Strain Ratio (PSR)

Due to the plane strain assumption that the diaphragm wall deflection in out-of-plane direction should be uniform, the result of two dimensional finite element analysis in deep excavation tends to be too conservative, especially in narrow but deep excavations.

Ou et al. (1996) used two and three dimensional finite element models to simulate the wall deflections in excavations of different distance from the corner, primary wall and complementary wall length.

They defined plane strain ratio (PSR) as the ratio of the maximum wall displacement of a section in the three dimensional analysis to the maximum wall displacement of a section under plane strain condition. From the result shown in Fig. 2.4 and Fig. 2.5, the conclusions were made that the deflections of short primary wall affected by distance to the corner heavily than longer primary wall does, while the longer primary wall is, the larger parts of wall would reach the plane strain condition. The chart of the length of secondary wall to the length of primary wall ratio versus distance from the corner was proposed (Fig. 2.6). The chart was divided into several zone by different plane strain ratios.

In addition, the convergence study was carried out before the large amount of numerical analyses. They found that the mesh density outside the excavation would be less significant than the mesh density inside.

Finno et al. (2007) took 50 finite element analyses with different subsurface conditions, wall stiffness and dimensions of excavations, as listed in Table 2.1 to Table 2.4, and obtain the following formula to estimate the PSR.

doi:10.6342/NTU201600809

$$PSR = \left(1 - e^{-\frac{kC}{L/H_e}}\right) + 0.05\left(\frac{L}{B} - 1\right)$$

where C is the factor depending on the factor of safety against basal heaving FS_{BH}:

$$C = 1 - [0.5(1.8 - FS_{BH})]$$

And k is the factor depending on the system stiffness S defined by Clough et al. (1989):

$$k = 1 - 0.0001S$$

$$S = \frac{EI}{\gamma_w h_{avg.}^4}$$

They concluded that when the ratio of the wall length to excavation depth $\frac{L}{H_e}$ is greater than 6, the PSR would be very close to 1, indicating that the wall behavior corresponds to plane strain condition. Furthermore, smaller $\frac{L}{B}$ ratio, stiffer wall systems and lower factor of safety against basal heaving would produce lower PSR. However, some other factors affecting the three dimension effects should be taken into consideration, such as struts type, prestress, ground water table and so on.

2.2 Relative system stiffness ratio

Bryson and Zapata-Medina (2012) used 48 models with different wall stiffness, vertical and horizontal spacing of struts, as listed in Table 2.5 to Table. 2.7, to propose a new system stiffness. The ground water table was assumed to be located at 3 meter below the ground surface and each struts were set 1 meter above excavation surface of last excavation all of the 48 models. They proposed a stiffness ratio called relative system stiffness R:

$$R = \frac{E_s}{E} \times \frac{S_H S_V H}{I} \times \frac{\gamma_s H_e}{s_u}$$

doi:10.6342/NTU201600809

where E_s is the Young's modulus of the soil; E is the Young's modulus of the wall. S_H and S_V are average horizontal and vertical spacing of struts respectively. I is moment of inertia per unit length of the wall. H is total height of the wall; H_e is excavation depth; s_u is undrained shear strength of the soil at the bottom of the excavation. The design chart of relative stiffness ratio was shown in Fig. 2.7.

They concluded that the design chart proposed by Clough et al (1989) tends to overestimate the lateral deformation in soft clay and underestimate it for stiff support systems in medium clay (Fig. 2.8).

doi:10.6342/NTU201600809

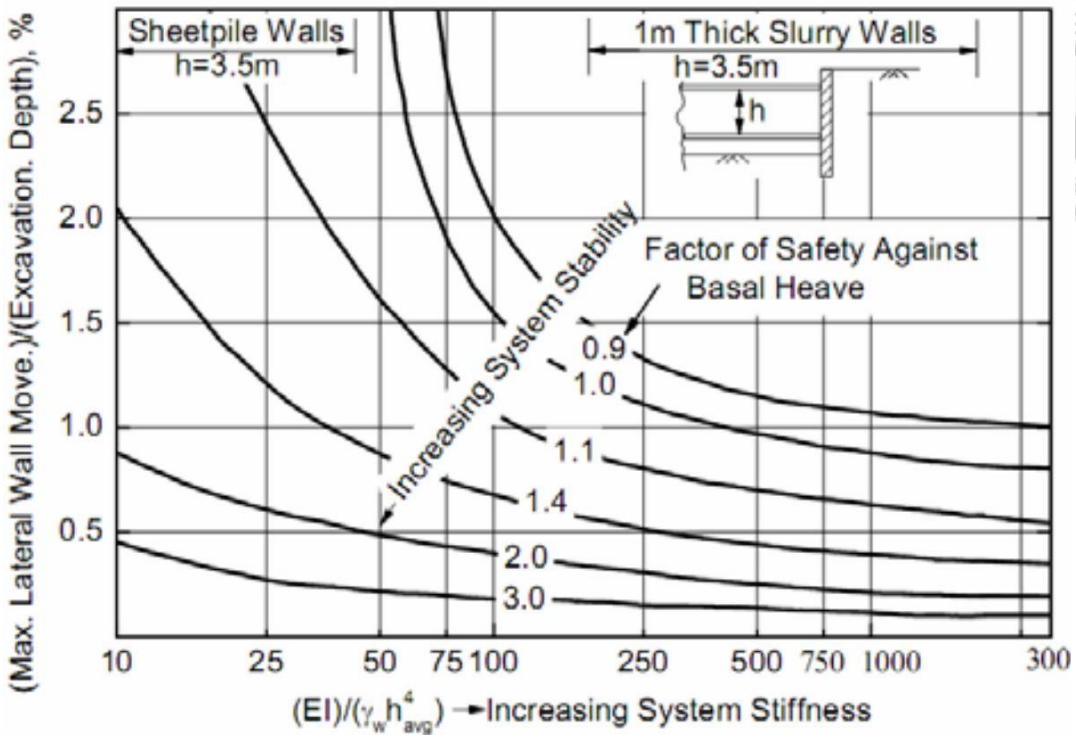

Fig. 2. 1 Design chart for estimating maximum lateral wall movement in soft to medium clays. (Clough and O'Rourke, 1990)

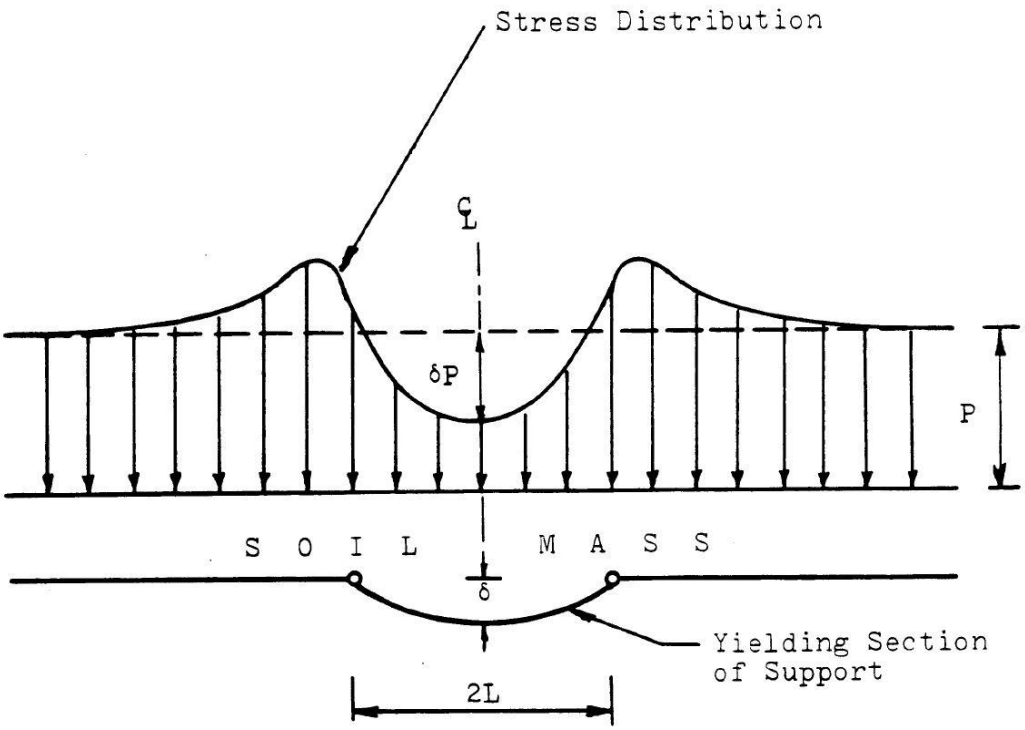

Fig. 2. 2 Distribution of soil stress while soil arching occurs. (Evans, 1984)

doi:10.6342/NTU201600809

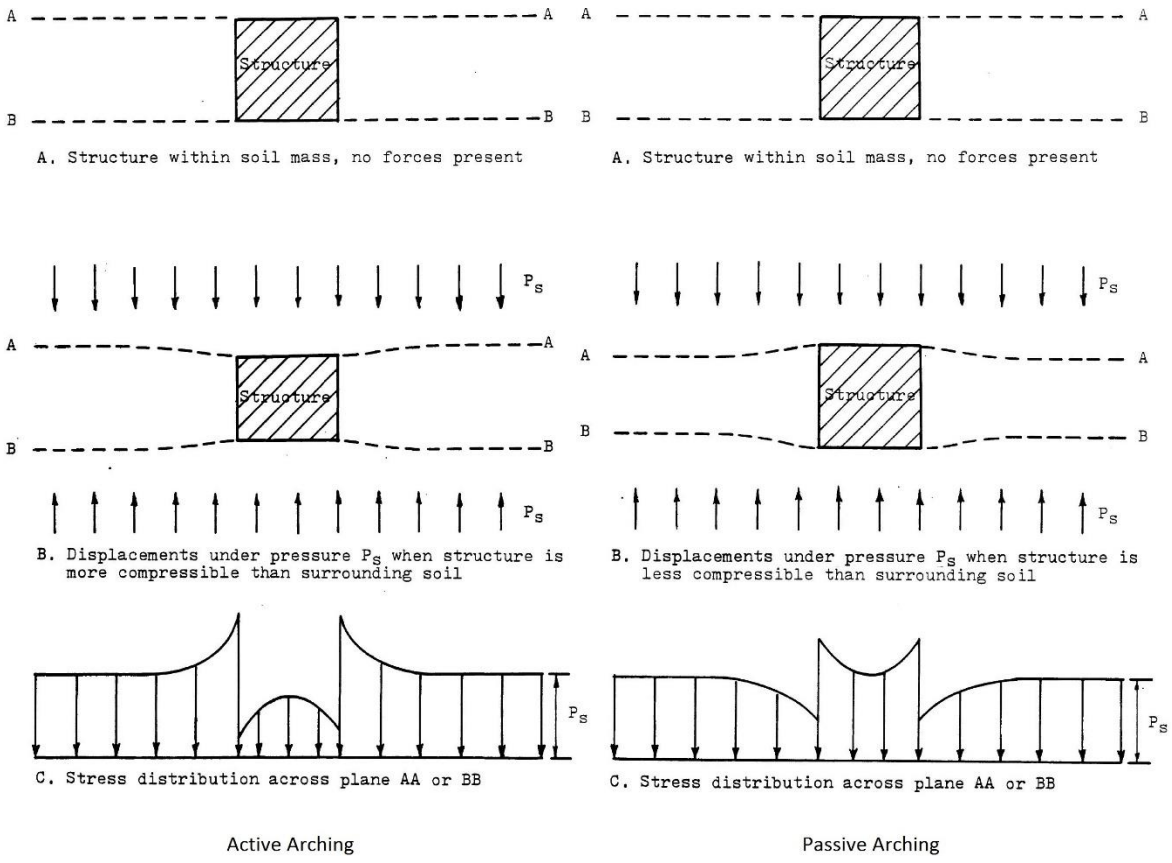

Fig. 2. 3 Distribution of soil stress in active and passive arching. (Evans, 1984)

doi:10.6342/NTU201600809

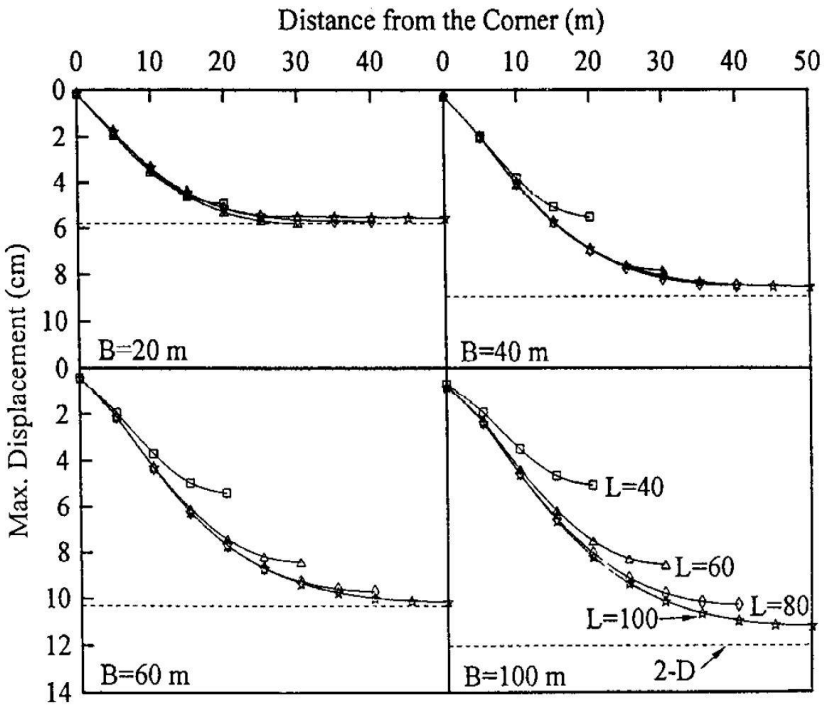

Fig. 2. 4 Variation of maximum wall displacement with the distance from the corner for constant sizes of complementary wall and various sizes of primary wall. (Ou, et al., 1996)

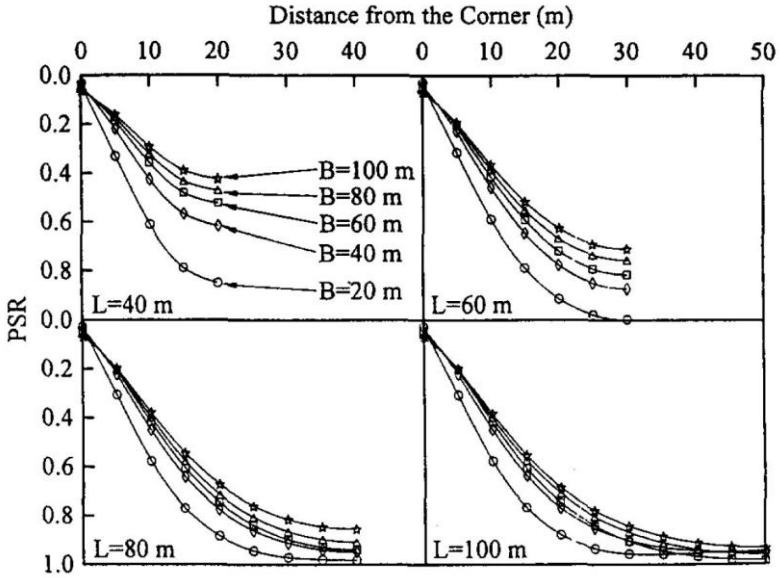

Fig. 2. 5 Variation of PSR for maximum wall displacement with the distance from the corner for constant sizes of primary wall and various sizes of complementary wall. (Ou et al., 1996)

doi:10.6342/NTU201600809

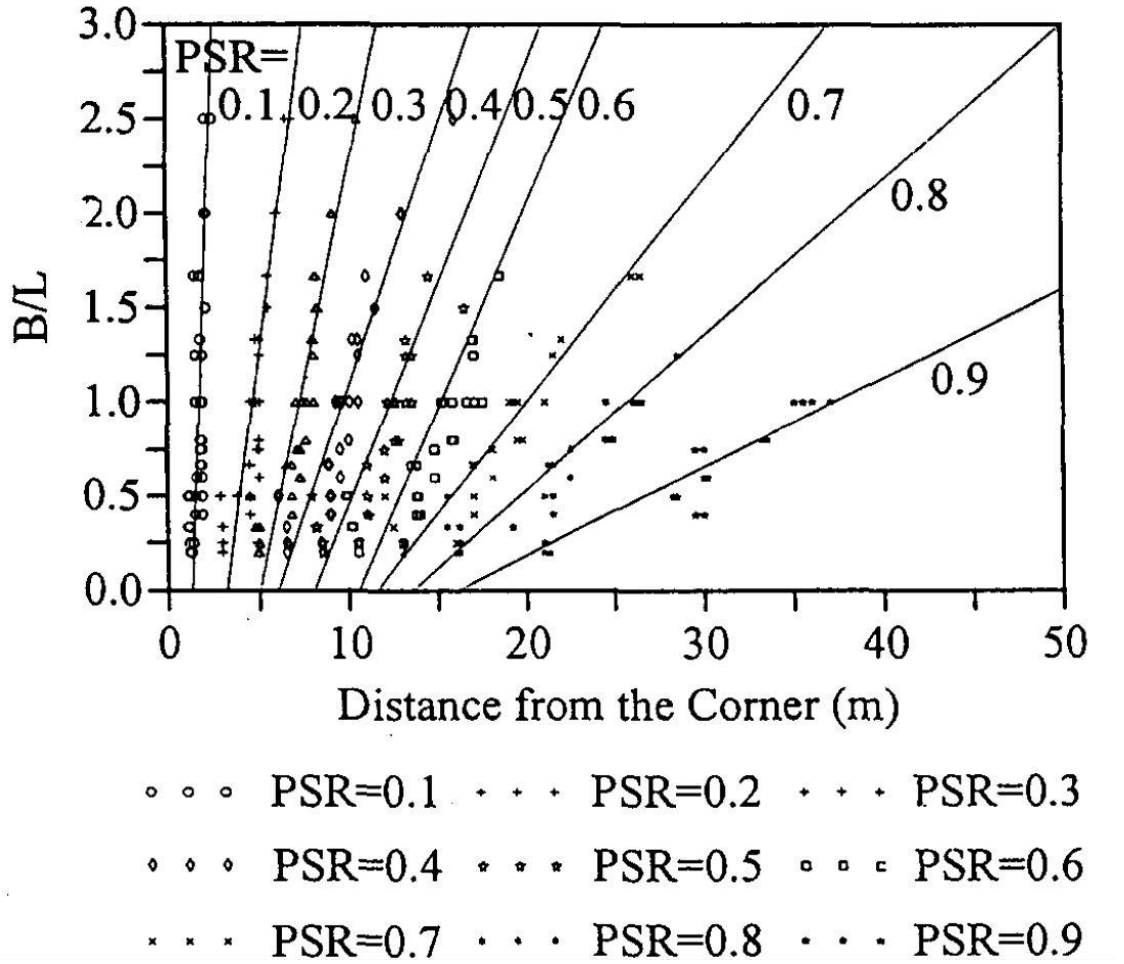

Fig. 2. 6 Relationship between ratio of complementary wall length to primary wall length and distance from corner for various PSR. (Ou et al., 1996)

doi:10.6342/NTU201600809

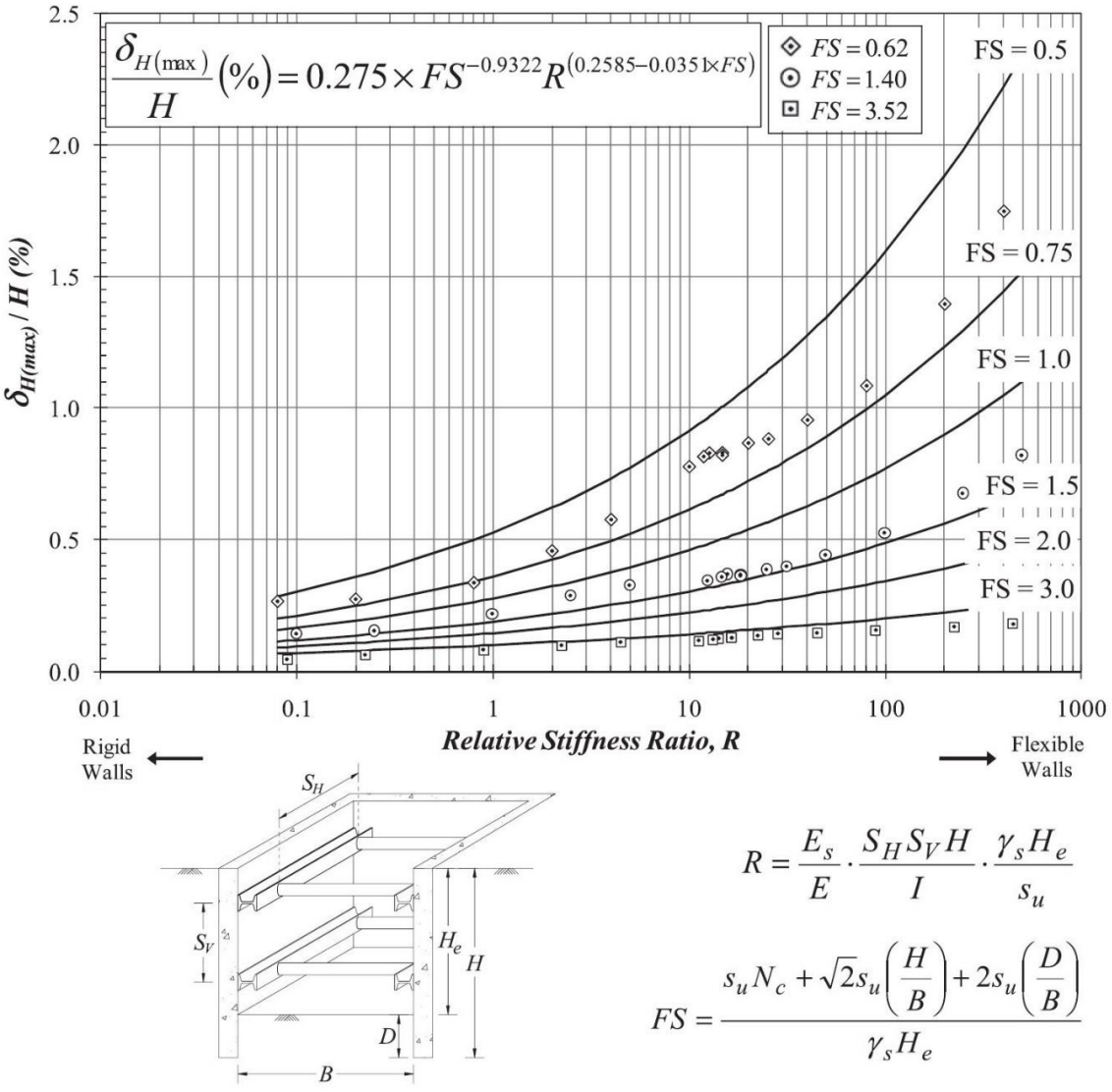

Fig. 2. 7 Relative stiffness ratio design chart. (Bryson et al., 2012)

doi:10.6342/NTU201600809

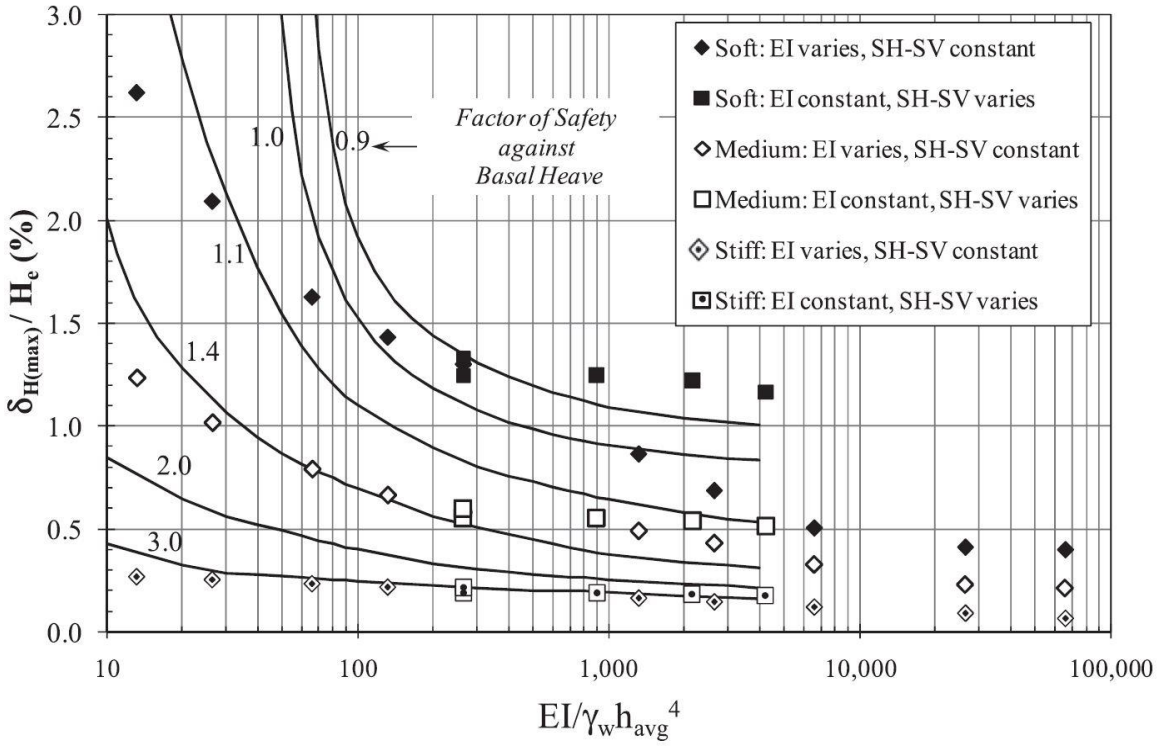

Fig. 2. 8 Comparison of the parametric studies with Clough et al. (1989) design chart.

(Bryson et al., 2012)

doi:10.6342/NTU201600809

Table 2. 1 Summary of three dimensional analyses. (Finno et al., 2007)

Stratum	H_e/FS_{BH}	L	B
A	9.8/1.7, 13.4/1.68, 16.3/1.8	20	20, 40, 80
		40	20, 40, 80
		80	20, 40, 80, 160[a]
		160	80[a]
B	9.8/1.63, 13.4/1.42, 16.3/1.28	20	20, 40
		40	20, 40, 80
		80	40, 80

[a] Analyzed for H_e equal to 9.8 m only.

Table 2. 2 Stratum conditions. (Finno et al., 2007)

	Elevation in Stratum A	Elevation in Stratum B
Sand	4.3 ~ -4.8 m	4.3 ~ -4.8 m
Soft Clay	-4.8 ~ -12 m	-4.8 ~ -14 m
Medium Clay	-12 ~ -14 m	-14 ~ -24 m
Stiff Clay	-14 ~ -24 m	N/A

doi:10.6342/NTU201600809

Table 2. 3 Hardening soil parameters. (Finno et al., 2007)

Parameters	Sand	Soft Clay	Medium Clay	Stiff Clay
E_{50}^{ref} (kPa)	7185	421	1284	17723
E_{oed}^{ref} (kPa)	7185	295	884	12406
c^{ref} (kPa)	1	1	1	1
Φ (°)	37	24	26	32
Ψ (°)	5	0	0	0
M	0.5	0.8	0.85	0.85

Table 2. 4 Parameters of wall. (Finno et al., 2007)

Parameters	Wall		
	Flexible	Medium	Stiff
Plane strain parameters			
System stiffness, S	32	320	3200
Bending stiffness, EI (MN-m^2/m)	50.4	504	5040
Axial stiffness, EA (MN/m)	3427	34270	342700
Thickness (m)	0.42	0.42	0.42
Poisson's ratio	0	0	0
Three dimensional parameters			
Young's modulus, E_1 (MPa)	8160	81600	816000
Young's modulus, E_2 (MPa)	408	4080	40800
Young's modulus, E_3 (MPa)	200000	2000000	20000000
Shear modulus, G_{12} (MPa)	408	4080	40800
Shear modulus, G_{13} (MPa)	400	4000	40000
Shear modulus, G_{23} (MPa)	1330	13300	133000
Thickness (m)	0.42	0.42	0.42
Poisson's ratio	0	0	0

doi:10.6342/NTU201600809

Table 2. 5 Summary of three dimensional analyses. (Bryson et al., 2012)

Model	Horizontal spacing of struts	Vertical spacing of struts	Stiffness of Wall
1	Various	Same as Model 1	Same as Model 1
2			
3			
4	Same as Model 1	Various	
5			
6			
7			
8		Same as Model 1	Various
9			
10			
11			
12			
13			
14			
15			
16			

doi:10.6342/NTU201600809

Table 2. 6 Hardening soil parameters for finite element modeling. (Bryson et al., 2012)

Parameters	Unit	Soft clay	Medium clay	Stiff clay
γ_{unsat}	kN/m^3	18.1	18.1	20
γ_{sat}	kN/m^3	18.1	18.1	20
$k_x = k_z$	m/day	0.00015	0.00015	0.00015
k_y	m/day	0.00009	0.00009	0.00009
E_{50}^{ref}	kN/m^2	2350	6550	14847
E_{oed}^{ref}	kN/m^2	1600	2380	4267
E_{ur}^{ref}	kN/m^2	10000	19650	44540
c_{ref}	kN/m^2	0.05	0.05	0.05
Φ	°	24.1	29	33
Ψ	°	0	0	0
ν_{ur}	N/A	0.2	0.2	0.2
p^{ref}	kN/m^2	100	100	100
Power	N/A	1.0	1.0	1.0
K_0^{nc}	N/A	0.59	0.55	1.5
$c_{increment}$	kN/m^3	0	0	0
y_{ref}	m	0	0	0
C_k	N/A	1.00E+15	1.00E+15	1.00E+15
R_f	N/A	0.7	0.95	0.96
T strength	kN/m^2	0	0	0
R_{interf}	N/A	1	1	1
δ -inter	m	0	0	0

doi:10.6342/NTU201600809

Table 2. 7 Wall rigidity values of each case. (Bryson et al., 2012)

Model	α	α*EI (kN-m^2/m)
1-7	1	540675
8	0.05	2703.75
9	0.1	54067.5
10	0.25	135168.75
11	0.5	270337.5
12	5	2703375
13	10	5406750
14	25	13516875
15	100	54067500
16	250	135168750

doi:10.6342/NTU201600809

doi:10.6342/NTU201600809

Chapter 3 Case Studies

The excavations in sandy soil are seldom studied in those research on the three dimensional effect in excavations. Therefore, the influence of three dimensional effect of excavations in sand are used as the subject of this study

Two case histories of foundation excavations located in Kaohsiung and Taipei, whose soil profiles are mainly consisted of sandy soil, were used as verifications of modeling framework. The results of three dimensional and two dimensional analyses were compared with in situ measurements.

3.1 Case A

Case A located in Kaohsiung, Taiwan, is a rectangular site with length of 70 m and width of 20 m. The depth of excavation is 16.8 m, implemented by the bottom-up construction method and retained by diaphragm wall with thickness of 0.9 m and 32 m deep. There are 5 stages of excavation and the diaphragm walls were propped by struts at 4 levels. The relative positions of each excavation surfaces, struts, and soil layers are shown in Fig. 3.1, while the soil profile are shown in Table 3.1. There were 4 inclinometers set in the middle of each side of diaphragm wall to monitor the wall deformation, as indicated in Fig. 3.2, and the measurements of inclinometer are shown in Fig. 3.3. Construction site information and in situ measured data in Case A were obtained from Dao (2015).

The raw measured inclinometer data are slopes of diaphragm wall at different depth, and the toes of diaphragm wall were usually adopted as the reference points of the measurements of inclinometers. As can be seen in the Fig.3.3, the deflections of toes are zeros. According to Hwang et al. (2007), the connecting points where the first or

doi:10.6342/NTU201600809

second level of struts jointed the diaphragm wall are more stable than the toe, and they are more suitable to be the reference points of inclinometer measurements. Therefore, the correction method following by Hwang et al. was applied to Case A, shown in the Fig. 3.4.

As can be seen in Table 3.1, soil types of Case A are primarily sand except three thin clayey layers. It is concluded that sandy layers would dominate the behavior of wall deformation in Case A. The Mohr-Coulomb model was used and the parameters of the soil model are listed in Table 3.2 on the basis of Dao (2015). In the Table 3.2, the effective Young's modulus of sand was decided by following equation after Hsiung (2009).

$$E' = 2000N(kPa)$$

where N is the blow number of standard penetration test (SPT). The undrained Young's modulus of clay layer can be obtained by the following empirical equation as reported by Bowles (1996), Lim et al. (2010), Likitlersuang et al. (2013), Khoiri and Ou (2013).

$$E_u = 500S_u$$

Three finite element analyses were carried out, including 1 three dimensional model and 2 two dimensional models for different sections, shown in Fig. 3.5. The sections of two dimensional simulations are shown in Fig. 3.5 b, c and d.

According to the displacement result of simulations shown in Fig. 3.6, apparently, three dimensional analysis have much better performance than two dimensional analyses, especially at the short sides of the excavation. It can be seen that the wall on the short side deflected larger than long side in two dimensional analyses. In the other words, two dimensional analyses would overestimate the maximum wall deflection severely on the short side. This results of the analyses are considered reasonable, because plane strain condition was assumed is applied in two dimensional analyses, that

doi:10.6342/NTU201600809

is, the length of diaphragm wall in out-of-plane direction was assumed to be infinite long, the width of excavation, which is the distance of the walls in section in Fig. 3.5 b and c., became one of most important factor affecting the amount of wall deflections.

3.2 Case B

Case B is located in Taipei, Taiwan, with an irregular site shape and was constructed by the top-down method. There are 6 stages of excavation propped struts or floor slabs at 5 level (Fig. 3.7 and Fig. 3.8), and the soil profile is shown in Table 3.3. The longest side of Case B has a length of 50.5 m with a diaphragm wall thickness of 1 m and depth of 36 m. The excavation was 19.6 m deep. Case B is adjacent to Songshan-Xindan line and Zhonghe-Xinlu line of Taipei MRT system; therefore, the wall deflection was regulated by law strictly. According to "Regulation on Building Restrictions along MRT Facilities", the excavations near the MRT system must not cause any deflection of tunnel over 20 mm and deformation of rails over 10 mm. Therefore, Case B used much stiffer retaining system, including 16 wall piles to depth of 45 m, 4 buttress walls and 3 cross walls, as shown in Fig. 3.9.

The construction procedures of Case B are complicated. It was divided into two zones, MRT side and warehouse area (Fig. 3.9), with different excavation procedures shown in Fig. 3.7 and Fig. 3.8. There are 7 inclinometers set on each side of excavation (Fig. 3.9), where the measured deflections of the walls were shown in Fig. 3.10.

According to Hsieh et al. (2016), the diaphragm wall around SID 1 was co-constructed with four wall piles to bear the weight of superstructure, and the four inclined steel columns for the top-down construction method were designed. Therefore, it was observed that the diaphragm wall around SID 1 kept deflecting outward after the first stage of excavation.

doi:10.6342/NTU201600809

In Case B, the Mohr-Coulomb model were used with the parameters listed in Table 3.4. All of the site information and in situ measured data in Case B were provided by Trinity Foundation and Engineering Consultants, Co. Ltd.

In additional to Plaxis 3D analysis, the one-dimensional elastoplastic foundation beams analysis software TORSA (Taiwan Originated Retaining Structure Analysis) was also used.

The results of wall deformations show in Fig. 3.11. The finite element model was simplified for accelerating computation in Case B, i.e. the co-construction of diaphragm wall and wall piles was set vertically, but it can still react to the three dimensional effect.

The measured data shown in Fig. 3.10 and Fig. 3.11 was not corrected due to lack of complete wall deformation data at each construction stage. Therefore, the inclinometer correcting method in Case A cannot be applied here. As mentioned earlier, the diaphragm wall deformed shape can be obtained by inclinometers, but its displacement depends on the reference point we selected. Therefore, the wall deformed curves were shifted to match the toe displacements for the result of TORSA and Plaxis 3D separately, as shown in Fig. 12 and Fig. 13. It can be seen that three dimensional finite element method still works better because the three dimensional effect was involved in

From the cases studies, the performance of the three dimensional finite element analysis is better than the two dimensional analysis. Therefore, a series of three dimensional finite element analyses were carried out on a simple deep excavation model to examine the effects of various factors in the next chapter.

doi:10.6342/NTU201600809

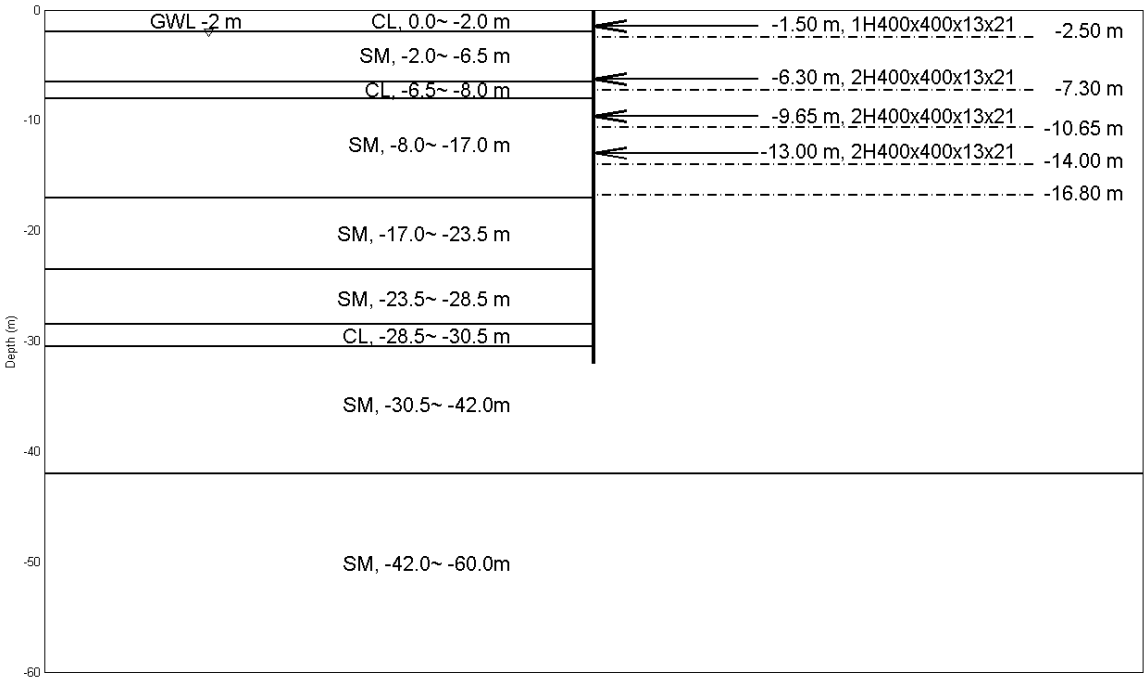

Fig. 3. 1 Cross section of retaining system and soil layers of Case A.

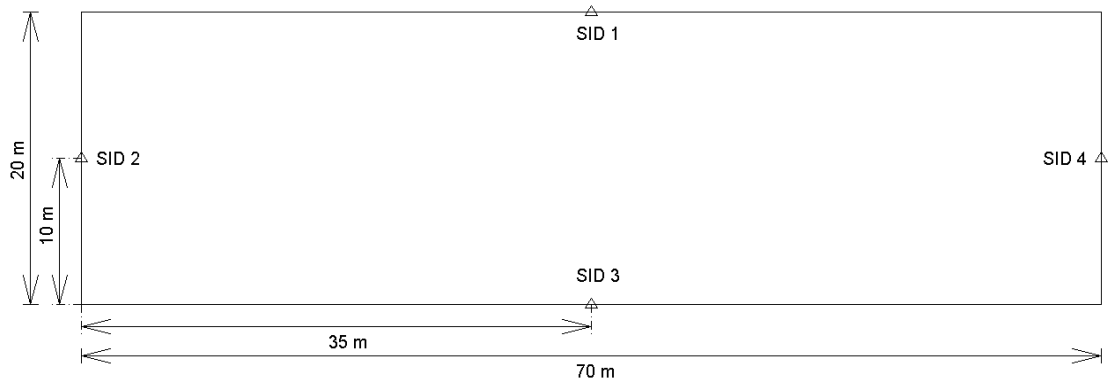

Fig. 3. 2 Plane view of monitoring equipment in Case A.

doi:10.6342/NTU201600809

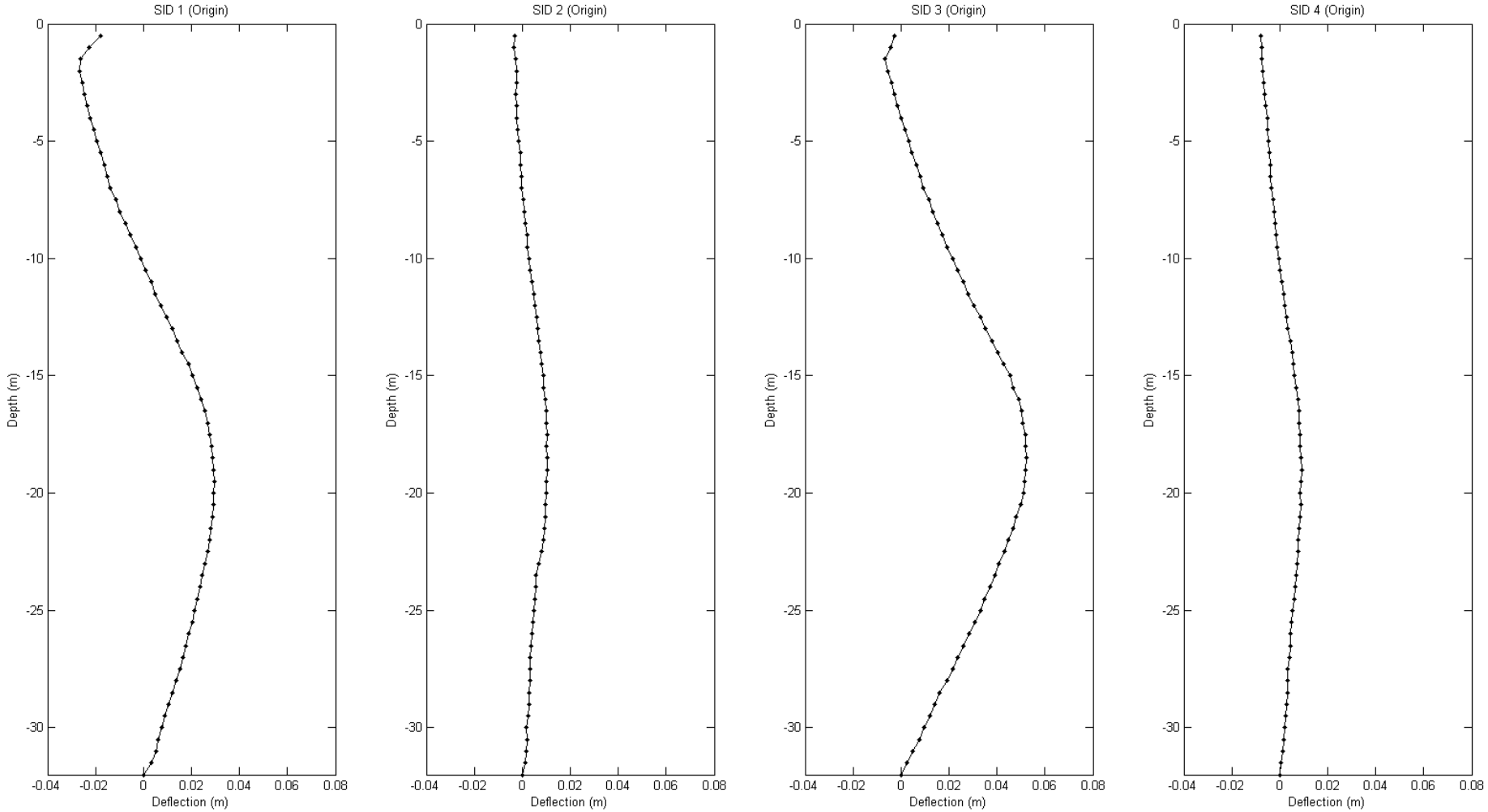

Fig. 3. 3 Wall deformations obtained by inclinometers in Case A.

doi:10.6342/NTU201600809

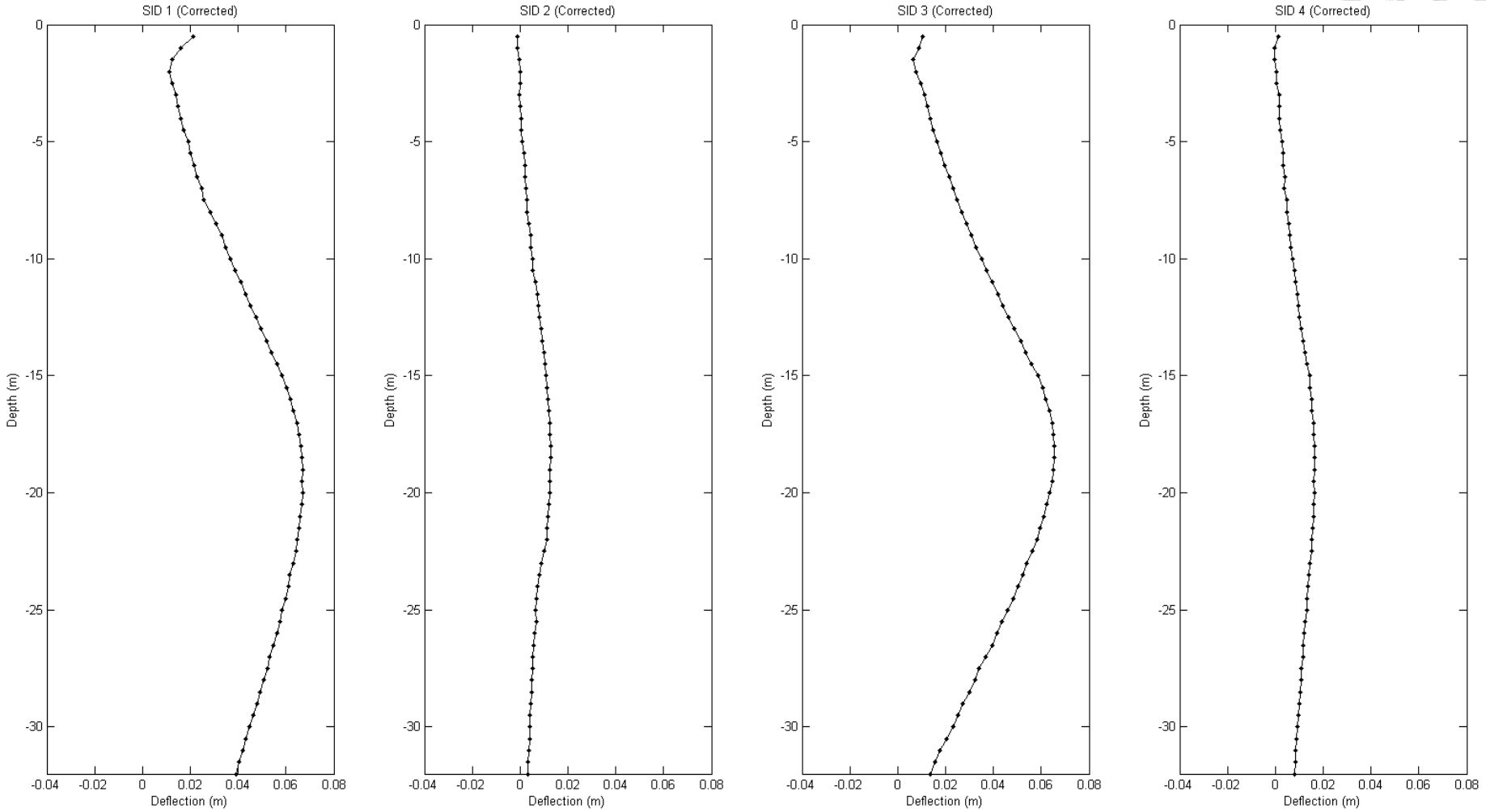

Fig. 3. 4 Corrected wall deformations obtained by inclinometers in Case A.

doi:10.6342/NTU201600809

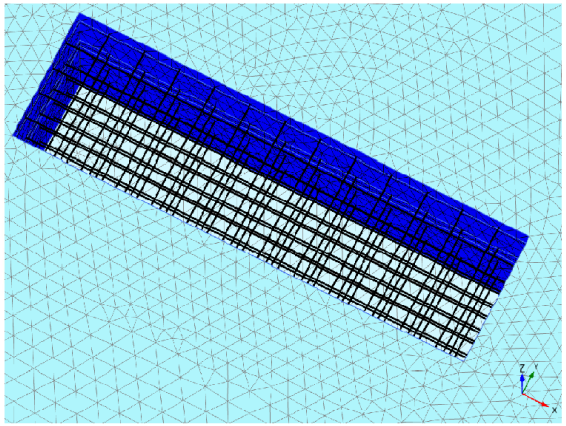

a. 3D model

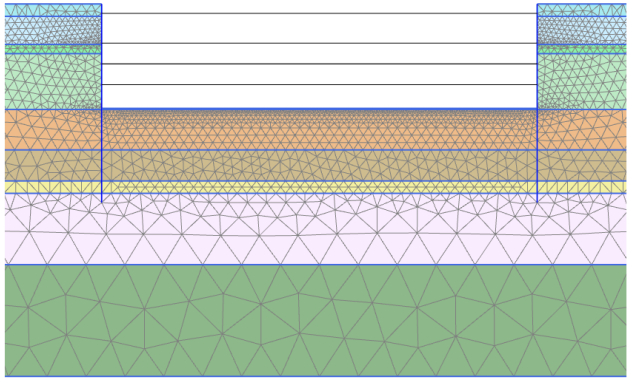

b. 2D model of short side section (section A–A')

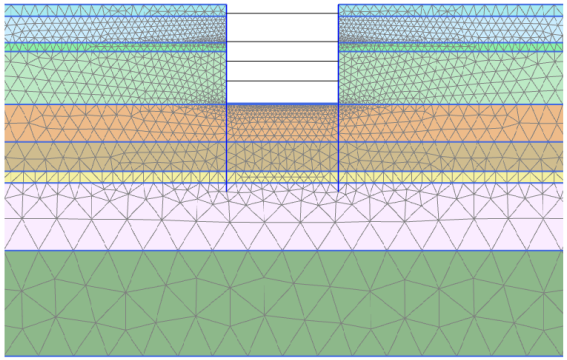

c. 2D model of long side section (section B–B')

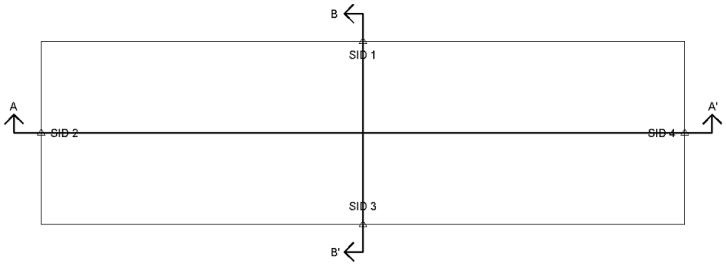

d. Section direction of 2D model

Fig. 3. 5 Finite element model of Case A.

doi:10.6342/NTU201600809

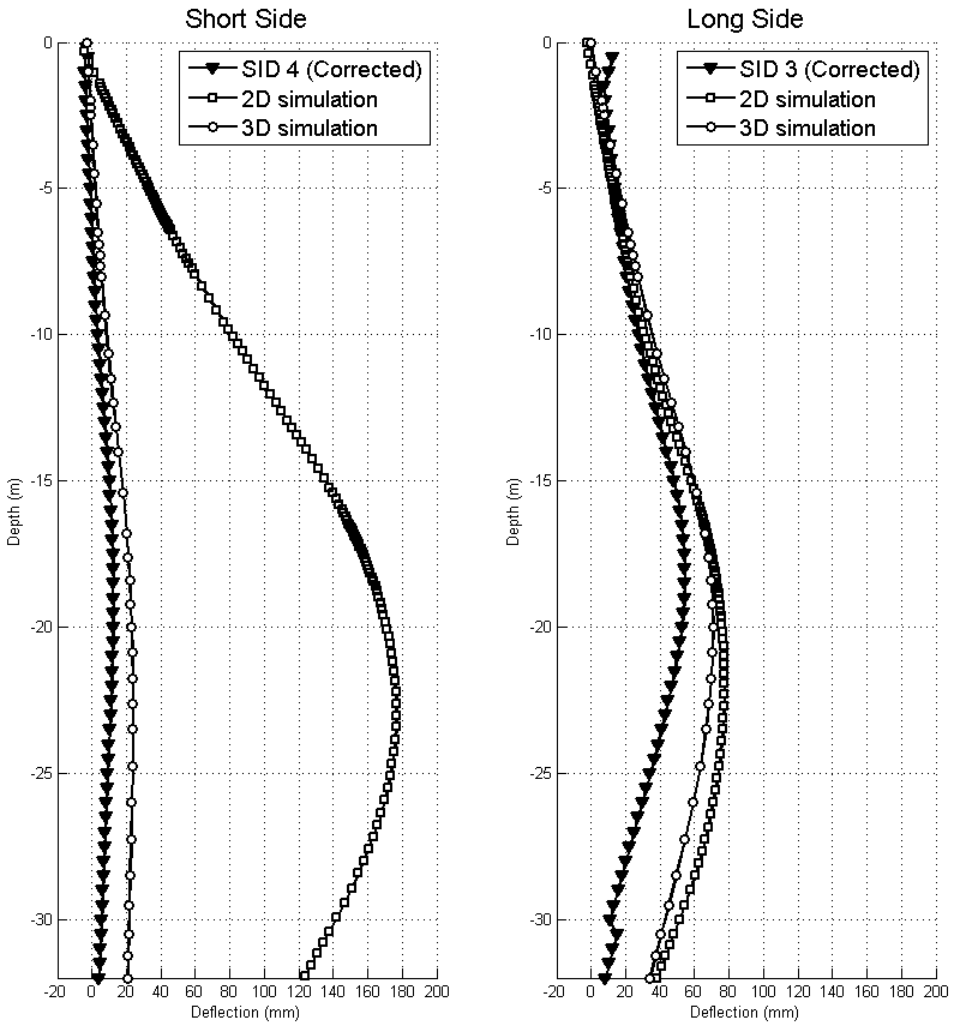

Fig. 3. 6 Wall deformations obtained by measurements and simulations in Case A.

doi:10.6342/NTU201600809

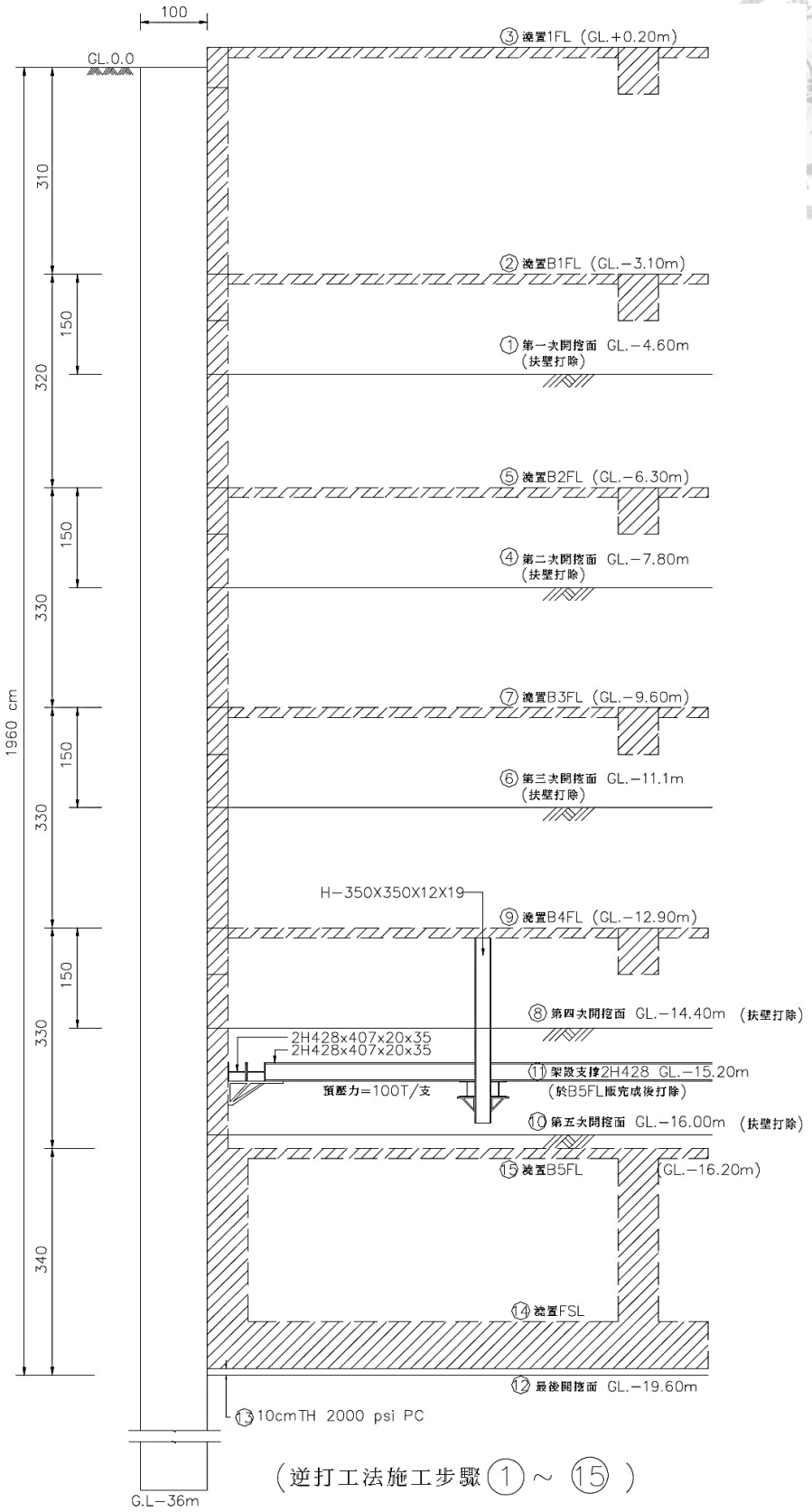

Fig. 3. 7 Cross sections of MRT side retaining system in Case B.

doi:10.6342/NTU201600809

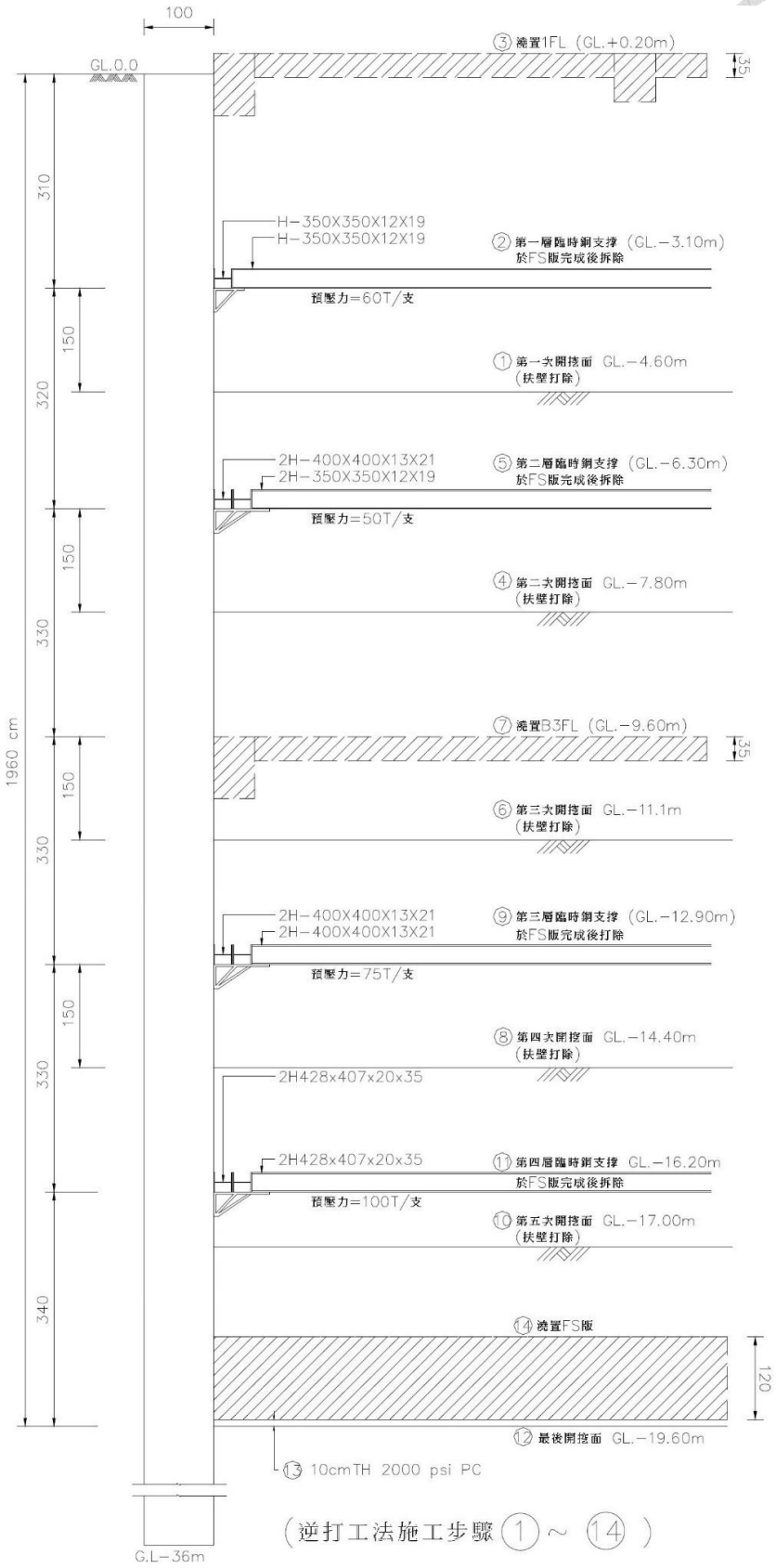

Fig. 3. 8 Cross sections of warehouse district retaining system in Case B.

doi:10.6342/NTU201600809

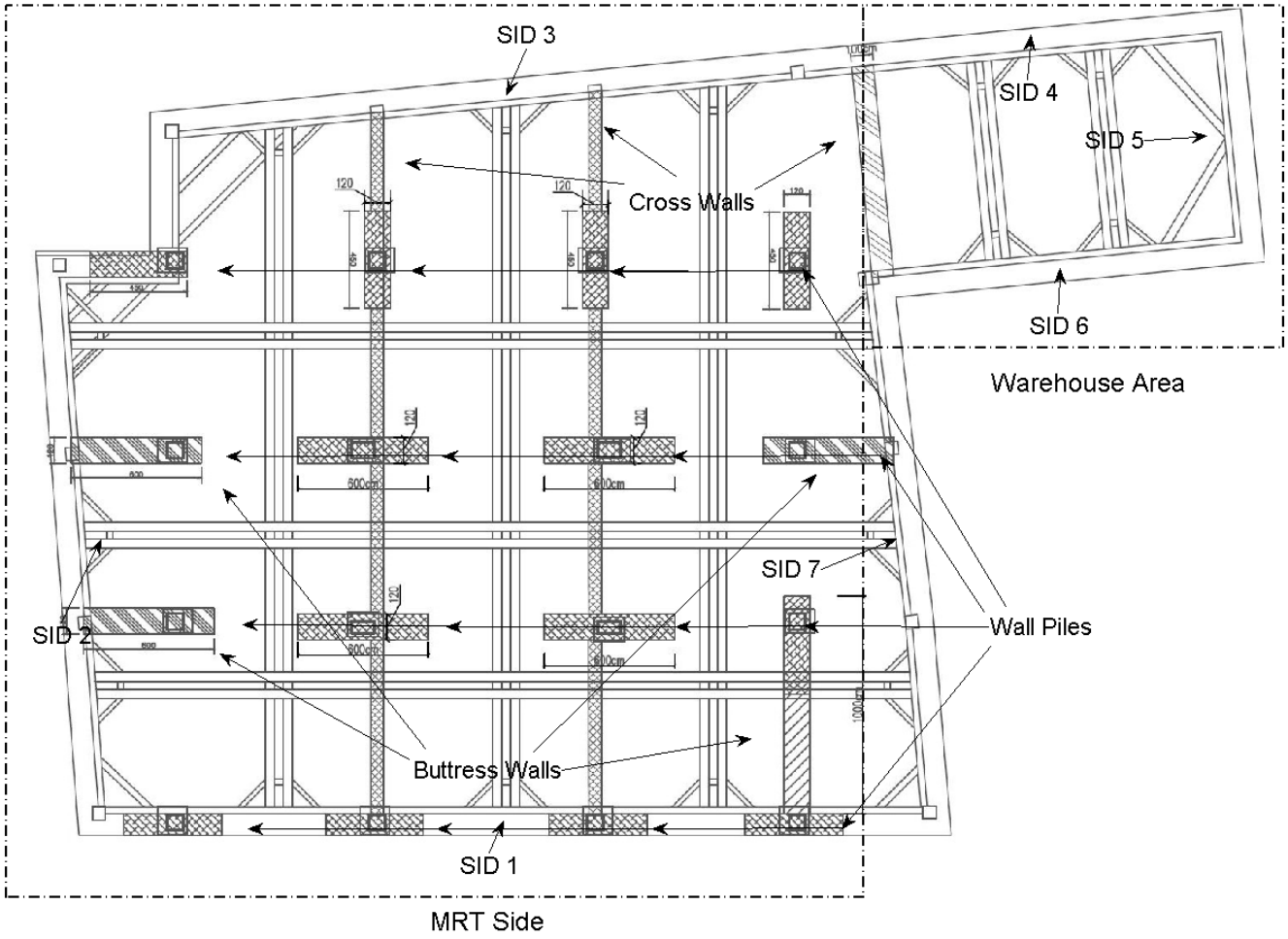

Fig. 3. 9 Plane view of Case B.

doi:10.6342/NTU201600809

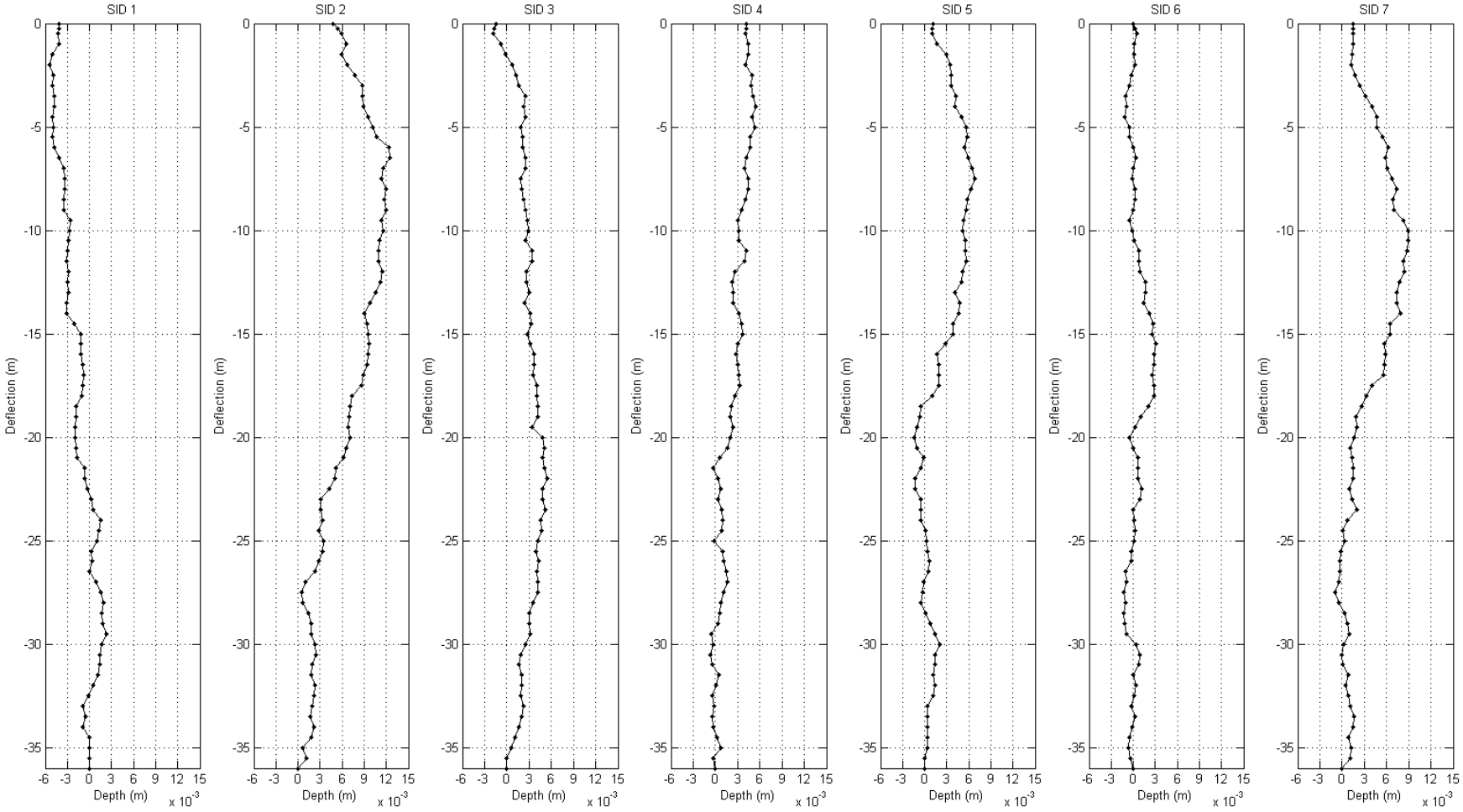

Fig. 3. 10 Wall deformations obtained by inclinometers in Case B.

doi:10.6342/NTU201600809

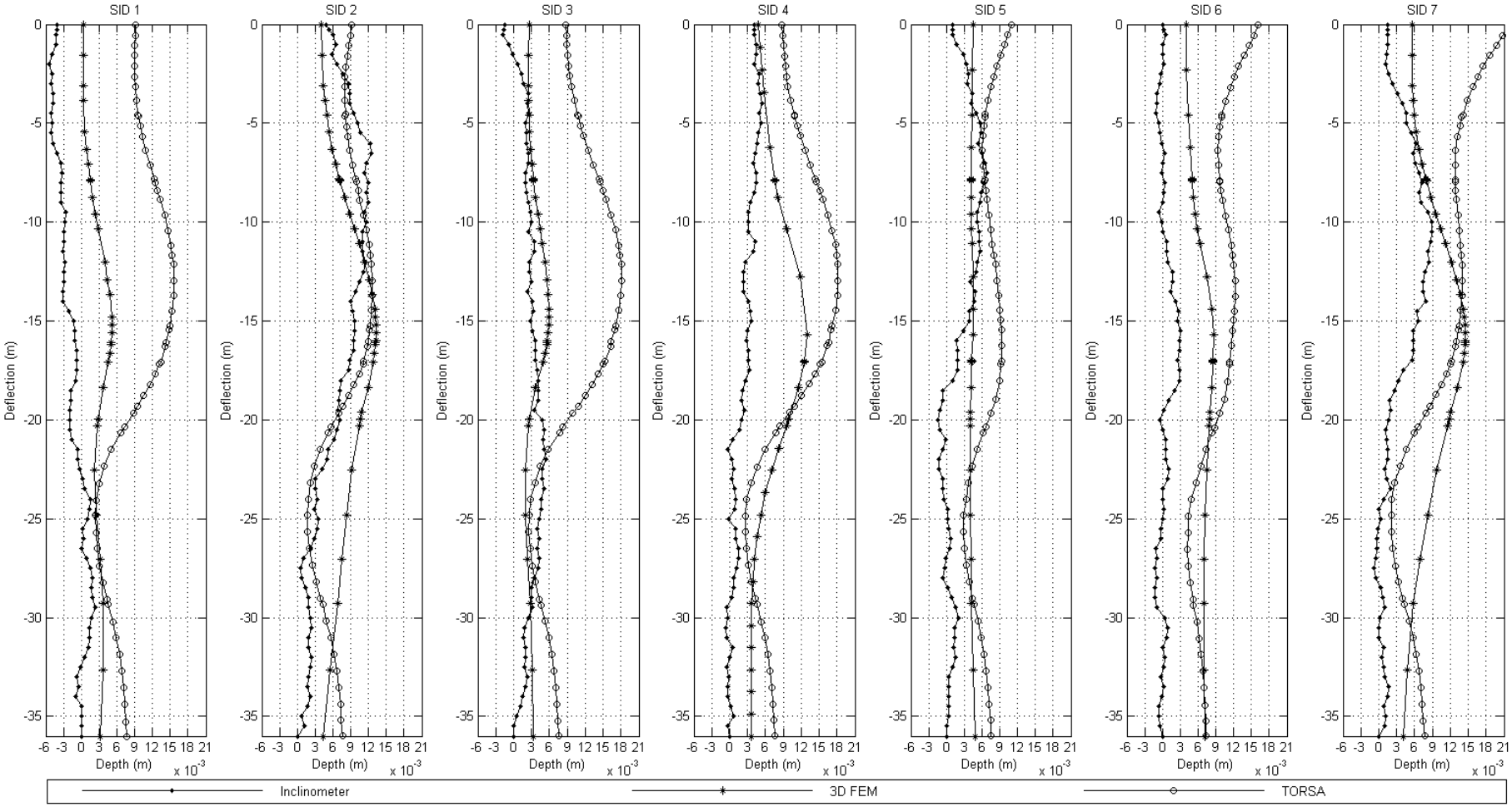

Fig. 3. 11 Wall deformations obtained by measurements and simulations in Case B.

doi:10.6342/NTU201600809

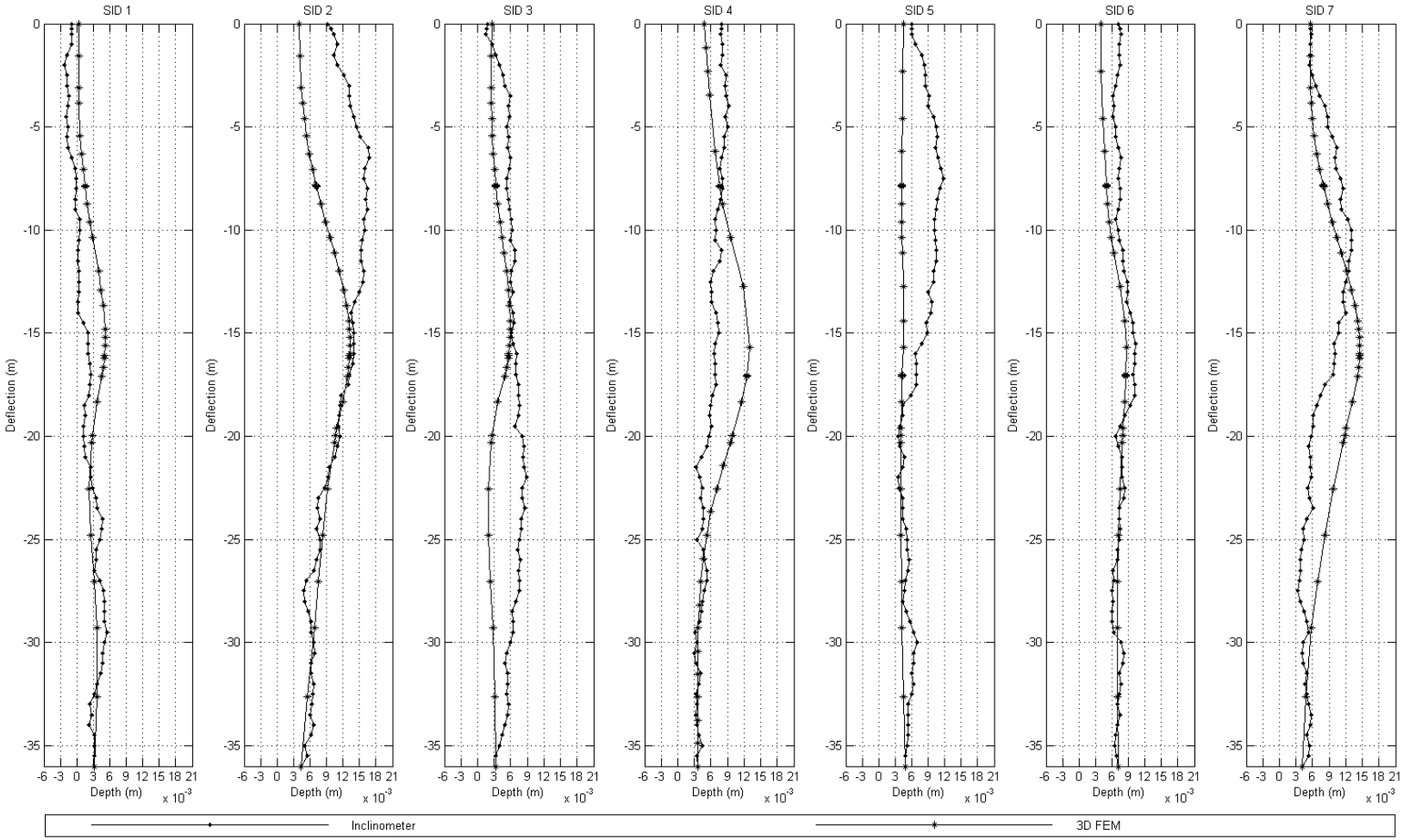

Fig. 3. 12 Wall deformations shifted to match Plaxis result.

doi:10.6342/NTU201600809

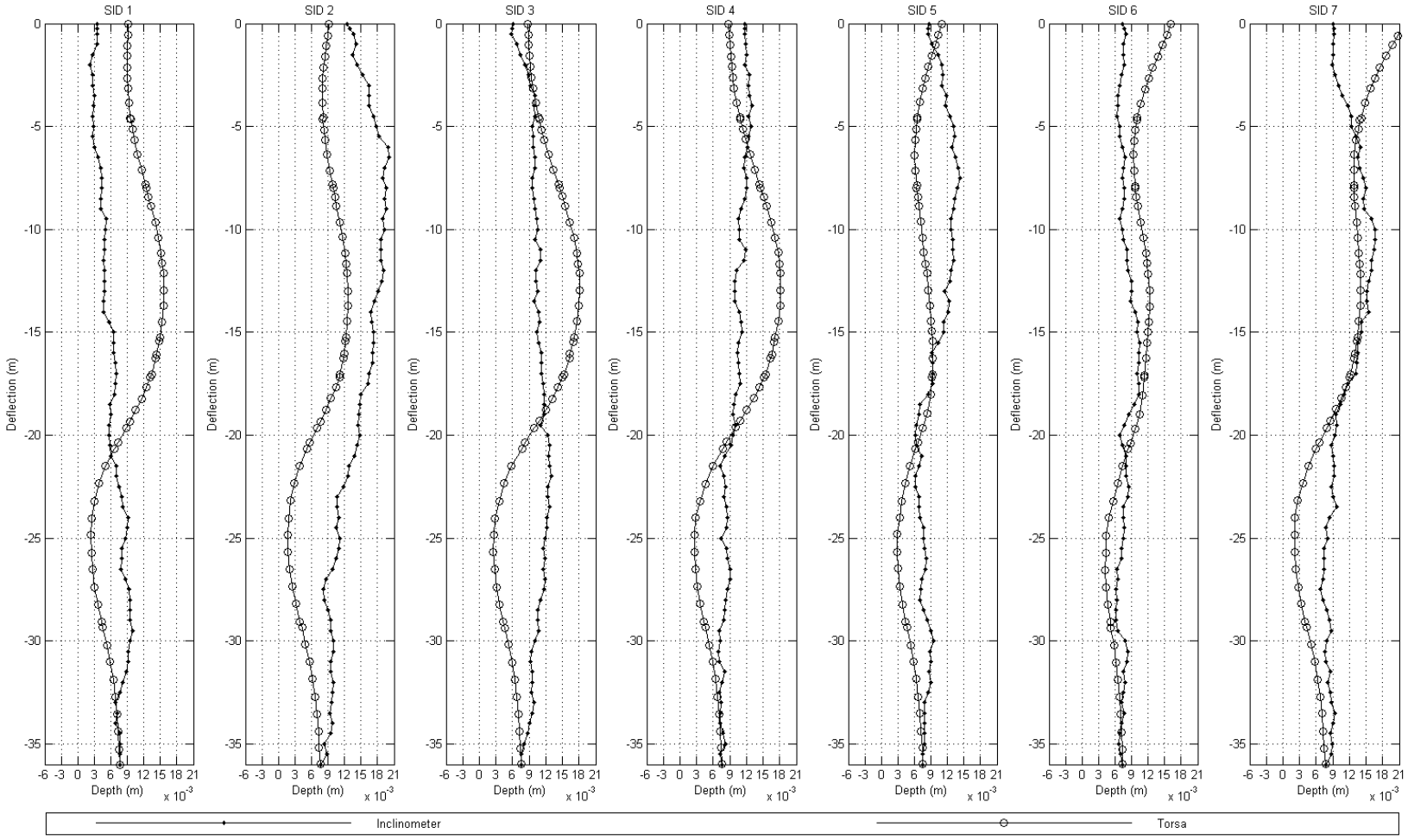

Fig. 3. 13 Wall deformations shifted to match TORSA result.

doi:10.6342/NTU201600809

Table 3. 1 Soil profile of Case A.

Depth (m)	Soil Type	γ_t (kN/m^3)	SPT N	φ’ (Deg)	c (kPa)
0.0-2.0	CL	19.3	6-7	29	28
2.0-6.5	SM	20.9	5-11	32	-
6.5-8.0	CL	19.7	3-4	30	21
8.0-17.0	SM	20.6	5-17	32	-
17.0-23.5	SM	18.6	5-17	32	-
23.5-28.5	SM	19.6	5-17	33	-
28.5-30.5	CL	18.6	11-15	32	84
30.5-42.0	SM	19.6	18-26	34	-
42.0-60.0	SM	19.6	28-42	34	-

doi:10.6342/NTU201600809

Table 3. 2 Soil parameters of Case A for Mohr-Coulomb model.

Depth (m)	Soil Type	γ_t (kN/m^3)	φ' (Deg)	c (kPa)	E' (MPa)	υ'	ψ' (Deg)	K_0	S_u (kPa)	E_u (MPa)	υ_u
0.0-2.0	CL	19.3	-	-	-	-	-	-	28	14	0.495
2.0-6.5	SM	20.9	32	0.5	16	0.3	2	0.47	-	-	-
6.5-8.0	CL	19.7	-	-	-	-	-	-	21	10.5	0.495
8.0-17.0	SM	20.6	32	0.5	22	0.3	2	0.47	-	-	-
17.0-23.5	SM	18.6	32	0.5	22	0.3	2	0.47	-	-	-
23.5-28.5	SM	19.6	33	0.5	22	0.3	3	0.46	-	-	-
28.5-30.5	CL	18.6	-	-	-	-	-	-	84	42	0.495
30.5-42.0	SM	19.6	34	0.5	44	0.3	4	0.44	-	-	-
42.0-60.0	SM	19.6	34	0.5	70	0.3	4	0.44	-	-	-

doi:10.6342/NTU201600809

Table 3. 3 Soil profile of Case B.

Depth (m)	Soil Type	γ_t (kN/m^3)	SPT N	φ' (Deg)	c (kPa)
0.0-7.9	CL	18.7	3-7	30	24.5-34.3
7.9-17.1	SM	19.4	11-24	32	-
17.1-20.3	CL	18.9	4-12	30	63.8
20.3-29.3	SM	19.2	10-38	33	-
29.3-39.5	CL/ML	18.6	9-23	32	117.7
39.2-41.4	SM	19.7	22-26	33	-
41.4-	GW	21.1	50	38	-

doi:10.6342/NTU201600809

Table 3. 4 Soil parameters of Case B for Mohr-Coulomb model.

Depth (m)	Soil Type	γ_t (kN/m^3)	φ' (Deg)	c (kPa)	E' (MPa)	υ'	ψ' (Deg)	S_u (kPa)	E_u (MPa)	υ_u
0.0-7.9	CL	18.7	30	0	-	-	-	24.5-34.3	19.6	0.495
7.9-17.1	SM	19.4	32	-	39.2	0.3	2	-	-	-
17.1-20.3	CL	18.9	30	0	-	-	-	63.8	34.3	0.495
20.3-29.3	SM	19.2	33	-	49.1	0.3	3	-	-	-
29.3-39.5	CL/ML	18.6	32	0	-	-	-	117.7	54.0	0.495
39.2-41.4	SM	19.7	33	-	61.3	0.3	3	-	-	-
41.4-	GW	21.1	38	-	122.6	0.3	8	-	-	-

doi:10.6342/NTU201600809

Chapter 4 Geometry Study

Eight factors, including excavation depth, wall depth, thickness of wall, length and width of excavation, difference of water head between inside and outside of excavation, average horizontal and vertical spacing of struts play significant roles in system stiffness of a deep excavation when three dimensional effect is considered.

Except for the factors mentioned above, other factors remained constant during analyses. In all of the geometry study, only single-layered sandy stratum was used and the soil parameters were unchanging. The H beam with dimension of 300 mm × 300 mm × 10 mm × 15 mm was used in each level of struts and pre-stressed to 490.5 kN (compression). The details of soil, wall, and struts parameters are listed in the Table 4.1.

According to Roboski (2004), the boundaries were set $\pm 5H_e$ (five times the excavated depth) to eliminate the boundary effect. A denser mesh was used inside the excavation and looser on the outside, on the basis of Ou et al. (1996).

The setting value of each factor was explained in the following section.

4.1 The Geometry Parameters

4.1.1 Excavation Depth (H_e) and Wall Depth (H)

There are two groups, Groups A and B, for different H_e and H in geometry study. According to normal depth of excavation for commercial building in Taiwan, excavation depths were set 20 m in Group A. A typical depth excavation for commercial building in Taiwan is around 20 m. The ratio of wall depth to excavation depth in a range usually depends on the soil type of excavation, i.e. 1.7 to 2.0 for sandy soil, 2.2 to 2.5 for clayey soil, and about 1.6 for gravelly layer. Therefore, H was selected to be 40 m in Group A for sandy soil deposit.

doi:10.6342/NTU201600809

For the Group B, H_e = 30 m and H = 60 m were used. This group is used for figuring out the three dimensional effect more comprehensively, though H_e and H are seldom reaching that value in practice.

4.1.2 Average Horizontal (H_h) and Vertical Spacing of Struts (H_v)

The average vertical spacing of struts (H_v) is related to the number of excavation stages as the level of each strut is normally set 1 m above the previous stage of excavation. Therefore, the number of construction stages depends on H_v. The value of H_v were set as 2.73 m, 3.33 m, 4.29 m for Group A and 2.86 m, 3.33 m, 4 m for Group B.

The average horizontal spacing of struts (H_h) were set to be 4 m, 5 m and 6m for both groups, which are the most common spacing used in Taiwan. Because the length and width of excavation are not always dividable by H_h, the following formula was used to calculate the number of struts needed:

$$N = floor(L_w \div H_h)$$

where N is the number of struts and L_w is the length or width of the excavation, depends on which side is calculated. The operator "floor" is used to round down $(L_w \div H_h)$ to an integer.

The horizontal positions of struts were calculated following the equation.

$$R = L_w - S(N+1)$$

$$S = round\left(\frac{L_w}{N+1} \times 10\right) \div 10$$

where R is the horizontal distance from the corner to the closest struts, and S is the horizontal spacing between each strut. The operator "round" means round off to an integer. $\frac{L_w}{N+1}$ multiplied by 10 before round off and divided by 10 after round off

doi:10.6342/NTU201600809

could make S accurate to one decimal point.

As can be seen in the formulae above, the H_h would become L_w/N, but not equal to the H_h set previously. The H_h, after the processes above, is in the range between 2.67 m and 5.92 m for Group A and between 3 m and 5.94 m for Group B.

4.1.3 Maximum Water Head Difference (H_w)

In practice, the ground water table inside the excavation should be maintained about 1 m below the surface of the following excavation. The ground water table is about 2 m to 6 m below the ground surface in Taipei basin; therefore, the lowering of the ground water table inside the excavation is necessary. However, the dewatering would lead to a higher water head difference between the inside and the outside of the excavation, where the large water pressure would have the diaphragm wall deformed.

The final excavation surfaces are 20 m for Group A and 30 m for Group B, while the final ground water tables inside the excavation are 21 m and 31 m, respectively. The ratio of the maximum water head difference to the excavation depth $\frac{H_w}{H_e}$ were selected to be 0.95, 0.7 and 0.45. To simplify the model, the level of outer ground water table did not drop accordingly during the construction. Instead, it remained constant throughout the entire time.

4.1.4 Thickness of Wall (D)

The thickness of wall, in a typical design, is about 5 percent of the excavation depth. To examine the influence of the wall stiffness to the three dimensional effect, the wall of 0.5 m, 1.8 m and 1.2 m thick were used in the simulations.

4.1.5 Dimensions of Excavation (L and B)

All of the excavation sites in the geometry study were rectangular ones. L is the length of the primary wall and B is the length of the complimentary wall. In a three

doi:10.6342/NTU201600809

dimensional model, the primary and complimentary walls could be switched to obtained more simulation results. In other words, the primary wall is not always the longest one. It depends on which wall deformation is to be observed, and the complimentary wall is the one next to it.

In the work done by Finno et al. (2007), the three dimensional effect become insignificant when the ratio of the excavation length to depth ($\frac{L}{H_e}$) over 6. They also indicated that the excavation length to width ratio ($\frac{L}{B}$) has some influence on PSR. Therefore, $\frac{L}{B}$ and $\frac{L}{H_e}$ were used to determine the dimensions of excavation for the simulations.

Firstly, $\frac{L}{H_e}$ were set to be 0.5, 1.0, 1.5, 2.0, 2.5 and 3.0, respectively. Secondly, $\frac{L}{B}$ were set to be 0.5, 0.7, 1.1, 1.3 and 1.7. Therefore, 30 sets of excavation dimensions were determined. Considering the exchange of the primary and complimentary wall, $\frac{L}{H_e}$ and $\frac{L}{B}$ can vary from 0.29 to 6 and 0.5 to 2, respectively. More details on the dimensions of excavation can be seen in Table 4.2 and Table 4.3.

The factors mentioned above except L and B are shown more briefly in Fig.4.1, and the mesh density of finite element model could be seen in the Fig.4.2.

4.2 Results and Discussions

From Tables 4.2 and 4.3, there are 3 variations of the variables H_w, D, H_v, H_h, and 30 variations of dimensions in each group. A total number of 4860 different excavations were modeled in geometry study, which 9720 results on wall behaviors can be obtained.

To properly define a new system stiffness incorporating the three dimensional effect, the correlation analysis between each factor and the normalized wall deformation were conducted first. The initial value of power term for each factor depends on the

doi:10.6342/NTU201600809

correlation coefficient. Then the power terms were accordingly adjusted to optimize a convergence of the proposed equation for the system stiffness. After several trials, the proposed new system stiffness S_1 is formulated as follows.

$$S_1 = \log\left(\frac{H^{1.8} \times D^{2.1}}{H_e \times H_w^{2.8} \times L^{1.7} \times B^{0.8} \times H_v^{0.8} \times H_h^{0.9}}\right)$$

The effects of L and B were illustrated in Fig.4.3. The width of the excavation B depended on $\frac{L}{B}$. In the other words, B increased while L became greater. In order to minimize the effect of L, the ratio $\frac{B}{L}$ was used to clarify the effect of B. It can be seen from the vertical and horizontal positions of points that L has great influence on wall deformation and S_1 can distinguish various L clearly. In B, the influence is blurred, therefore a lower power term of B was given according to the correlation coefficient.

The horizontal and vertical spacing of struts, H_h and H_v, have relative lower influence on wall deformation. As can be seen in Fig.4.4, the vertical positions of points had not much differences with H_h and H_v changing. Therefore smaller power terms should be given.

The thickness of wall, D, and normalized maximum water head difference, $\frac{H_w}{H_e}$, had significant influence on wall deformation, shown in Fig. 4.5. However, the total result would diverge if the power terms were too large, especially $\frac{H_w}{H_e}$. The moment of inertia of diaphragm wall, $I = \frac{LD^3}{12}$, was used in numerator of the system stiffness defined by Clough et al. (1989), so we set the initial value of power of D to 3. There is no formula of system stiffness including $\frac{H_w}{H_e}$, hence the initial value of power of $\frac{H_w}{H_e}$ was set arbitrarily. Finally we started the processes of trial and error with those initial value.

Due to $\frac{H}{H_e}$ remain constant, the figures of H_e and H would be the same, hence

doi:10.6342/NTU201600809

only H_e was shown in Fig.4.6. For the same reason as $\frac{H_w}{H_e}$ H_e and H also needed the processes of trial and error with arbitrary initial value.

As the proposed system stiffness S_1 came out, a new design chart was plotted with S_1 versus the maximum deformation of wall normalized by excavation depth (Fig.4.7), the fitting result with sum of squared error (SSE) equals 43.32 and R-square equals 0.97 was also shown.

The proposed design chart was divided and re-colored by different factors to examine the performance. In Fig.4.8, the chart was divided into 3 parts with different range of L and colored by $\frac{B}{L}$. The darker color of markers represent the higher value of $\frac{B}{L}$. It was found that the darkest markers ($\frac{B}{L}$ =2.0) located in the lower part of stripe while L = 31 m to 60 m, but it changed to upper part of stripe as L = 64 m to 180 m. That is, there are some interactions between L and $\frac{B}{L}$.

Again, the chart was divided into 3 parts with different $\frac{H_w}{H_e}$ and colored by other factors, seen in Fig.4.9 to Fig.4.11. It can be seen that the distributions of other factors are quite the same in different $\frac{H_w}{H_e}$. In the other words, $\frac{H_w}{H_e}$ only affected how long the exponential tendency developed, but it had no interactions with other factors.

In Fig.4.7, the red point on left side represented the wall deformation on the long side of Case A, and the other represented the short one. Both of the sides followed the trend of geometry study, however the short one was nearly dropping beyond the trend. The regression equation overestimated the deformation about 9.96 mm and 32.11 mm on the long side and the short side, separately.

We thought the reason for overestimating the deformation on the short side and underestimating it on the long side is that the 9720 points for regression involving many

doi:10.6342/NTU201600809

extreme large and small cases, e. g. excavation with dimension of 90 m by 180 m retained by diaphragm wall with D = 0.5 m, H_v = 4 m and H_h = 6 m, and excavation with dimension of 10 m by 6 m retained by diaphragm wall with D = 1.2 m, H_v = 2.73 m and H_h = 2.67 m.

Those extreme cases would cause bias on the result of regression, especially the weight of each case in regression is equal, and therefore another proposed system stiffness S_2 came out. The definition of the proposed system stiffness S_2 was shown following:

$$S_2 = \log\left(\frac{H^{0.9} \times D^{2.7}}{H_e \times H_w^{3.5} \times L^{2.6} \times B^{0.8} \times H_v^{1.1} \times H_h^{1.1}}\right)$$

New regression analysis was conducted on those cases whose L is between 20 m and 71 m, shown in Fig.4.12. The fitting result with SSE equals 10.53 and R-square equals 0.98 was also shown.

It can be seen that the new regression equation worked better than the last one. The equation overestimated the wall deformation about 0.4 mm and 18.6 mm on the long side and short side, separately.

It should be noted that the regression results are only suitable for top-down excavations in sandy soil without cross wall and buttress wall due to the models used in this study.

doi:10.6342/NTU201600809

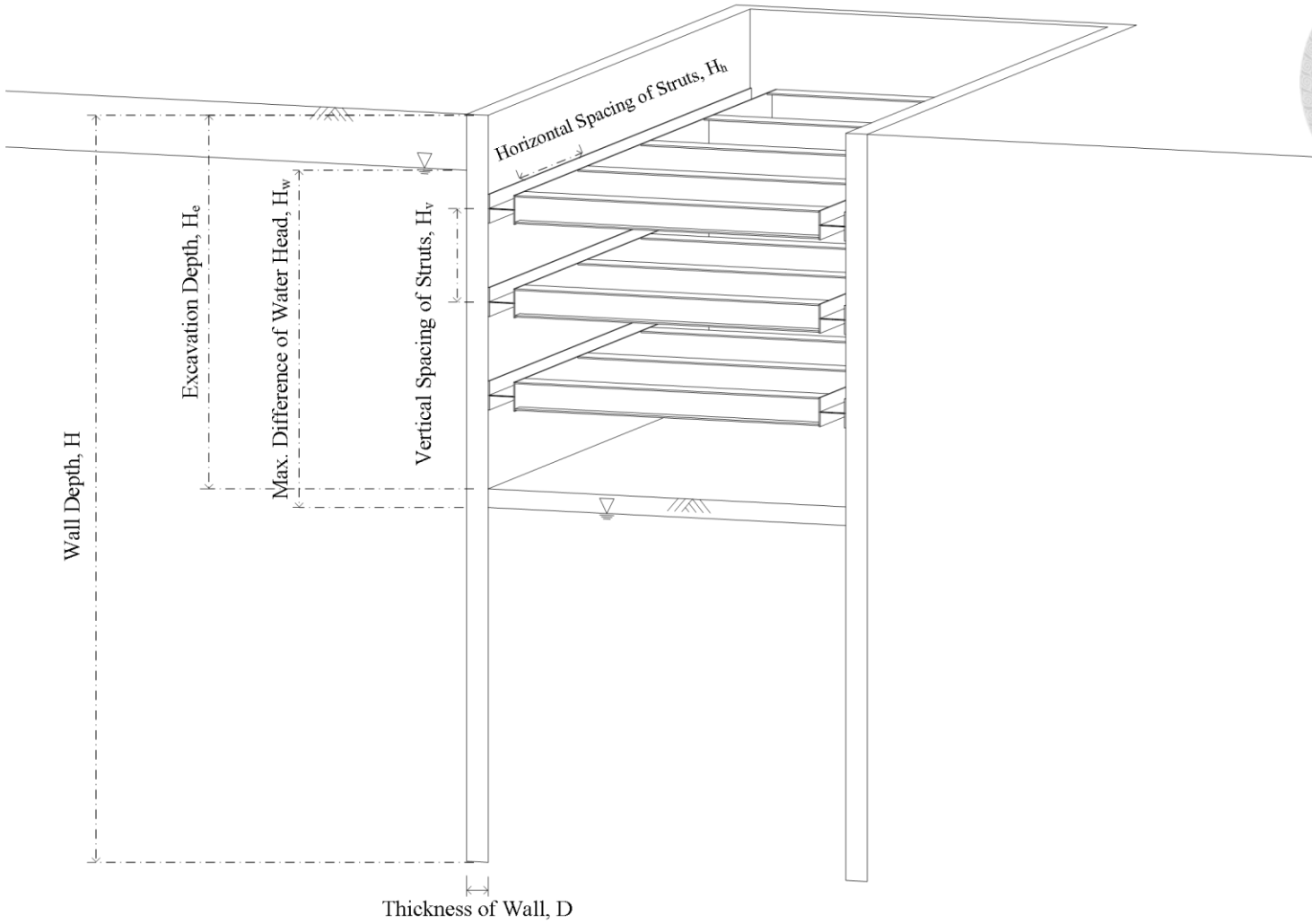

Fig.4. 1 Diagram of studied factors.

doi:10.6342/NTU201600809

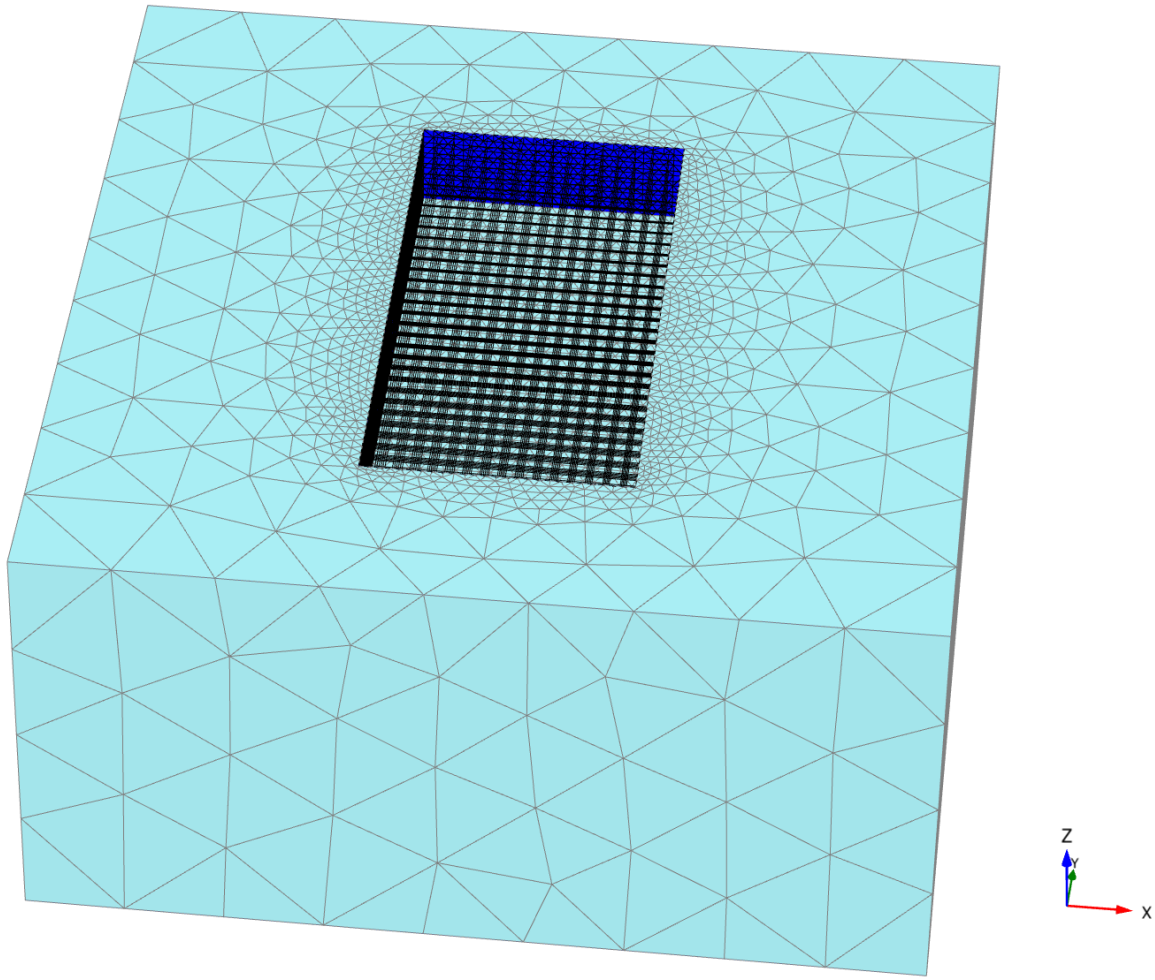

Fig.4. 2 The mesh density of finite element model.

doi:10.6342/NTU201600809

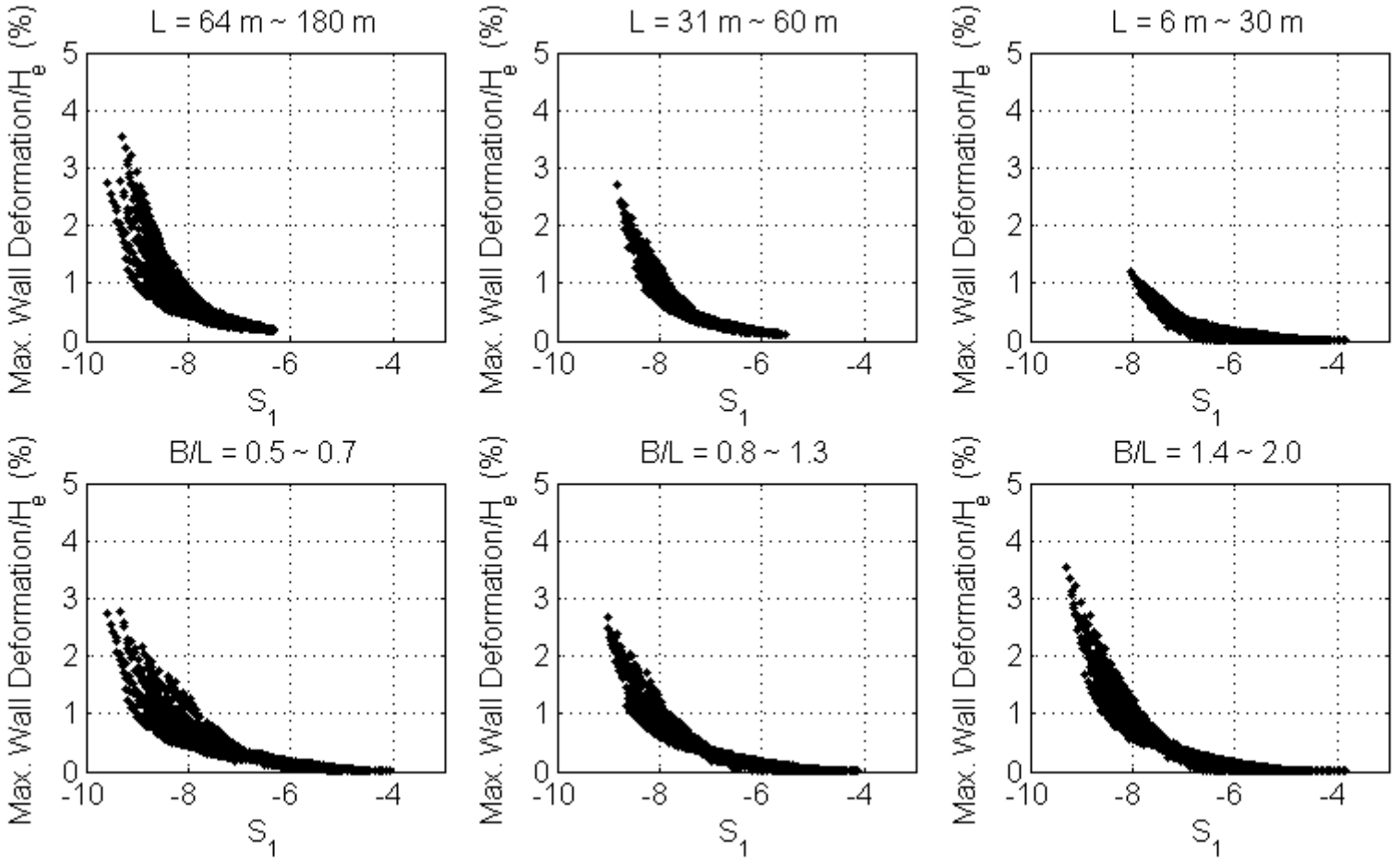

Fig.4. 3 The performance of S_1 on L and B/L.

doi:10.6342/NTU201600809

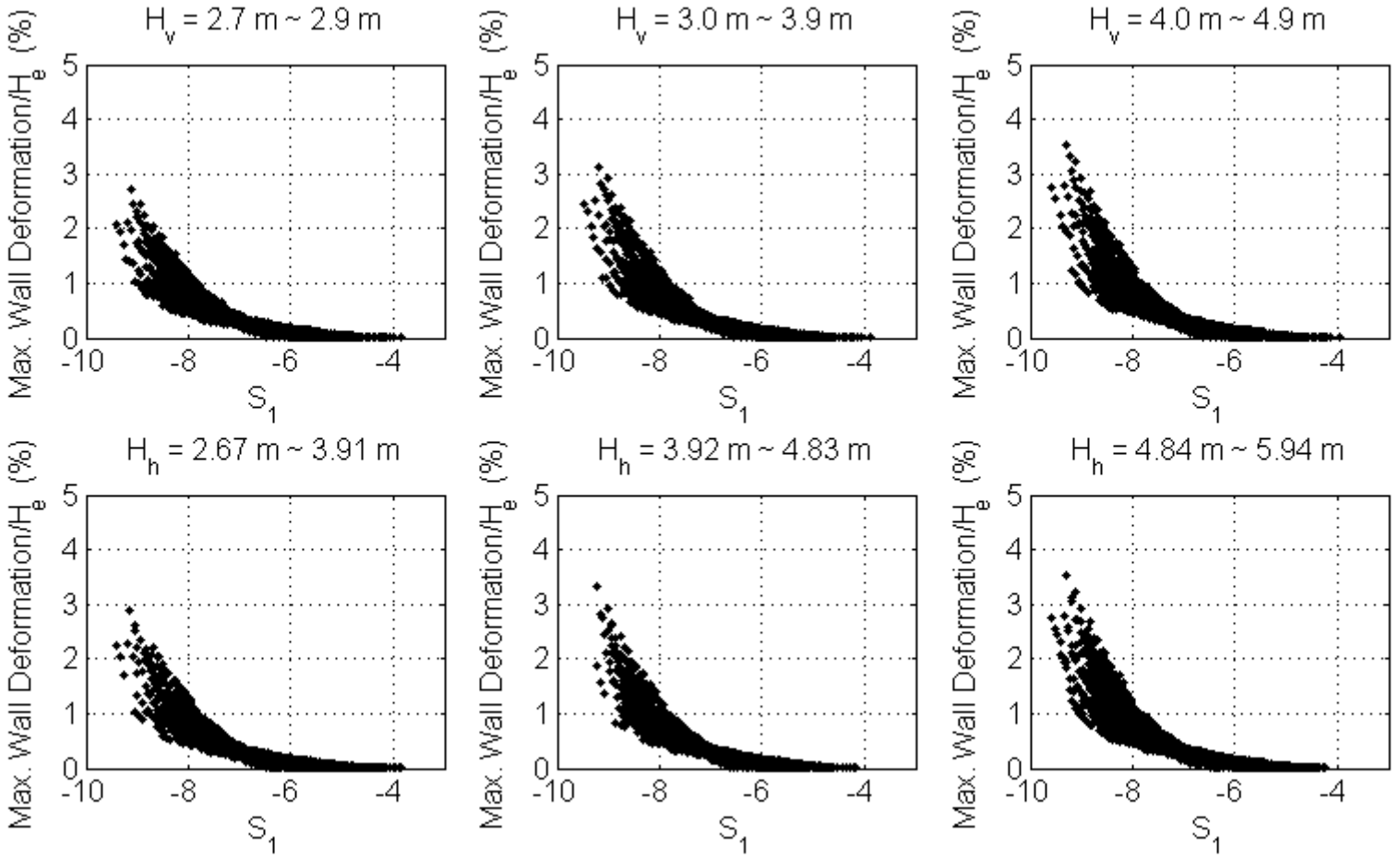

Fig.4. 4 The performance of S_1 on H_v and H_h.

doi:10.6342/NTU201600809

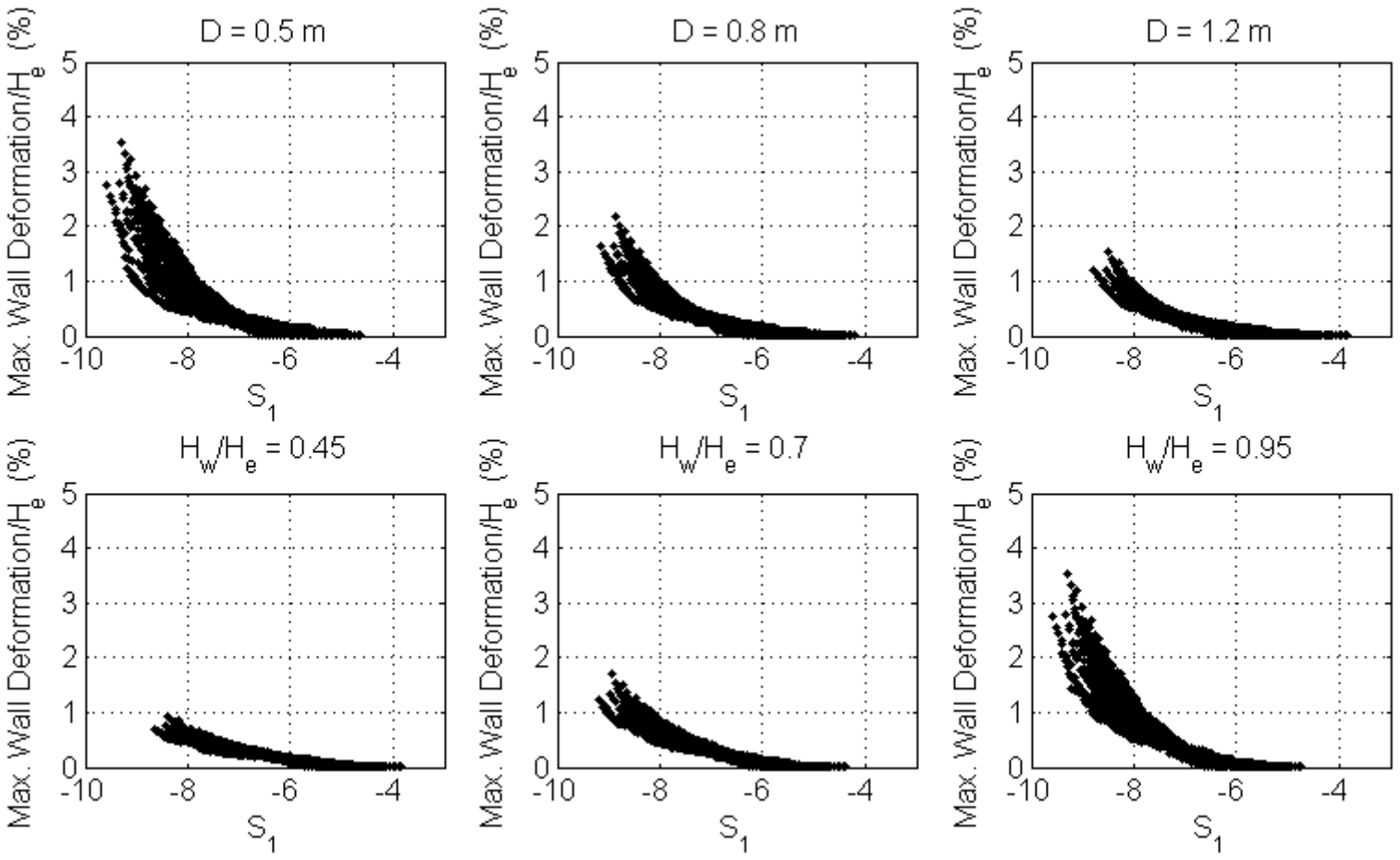

Fig.4. 5 The performance of S_1 on D and H_w/H_e.

doi:10.6342/NTU201600809

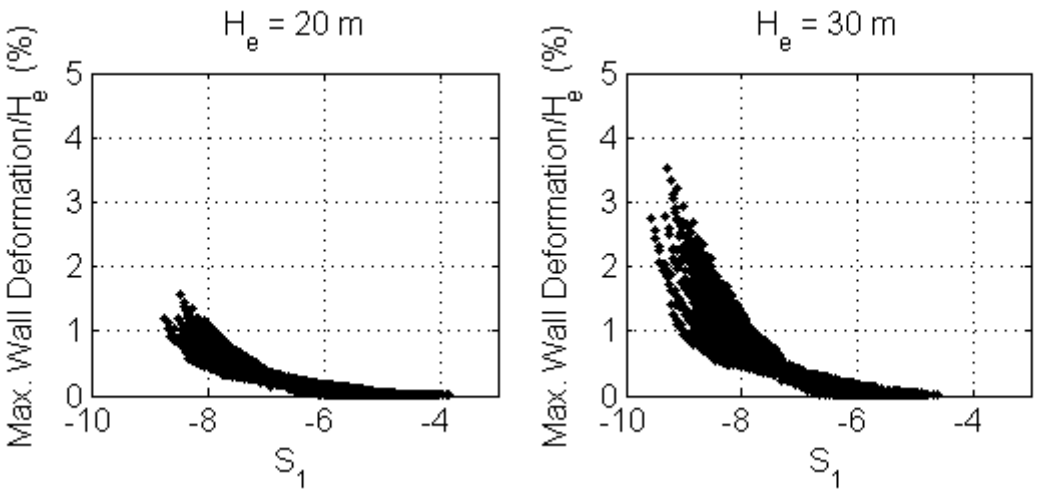

Fig.4. 6 The performance of S_1 on H_e.

doi:10.6342/NTU201600809

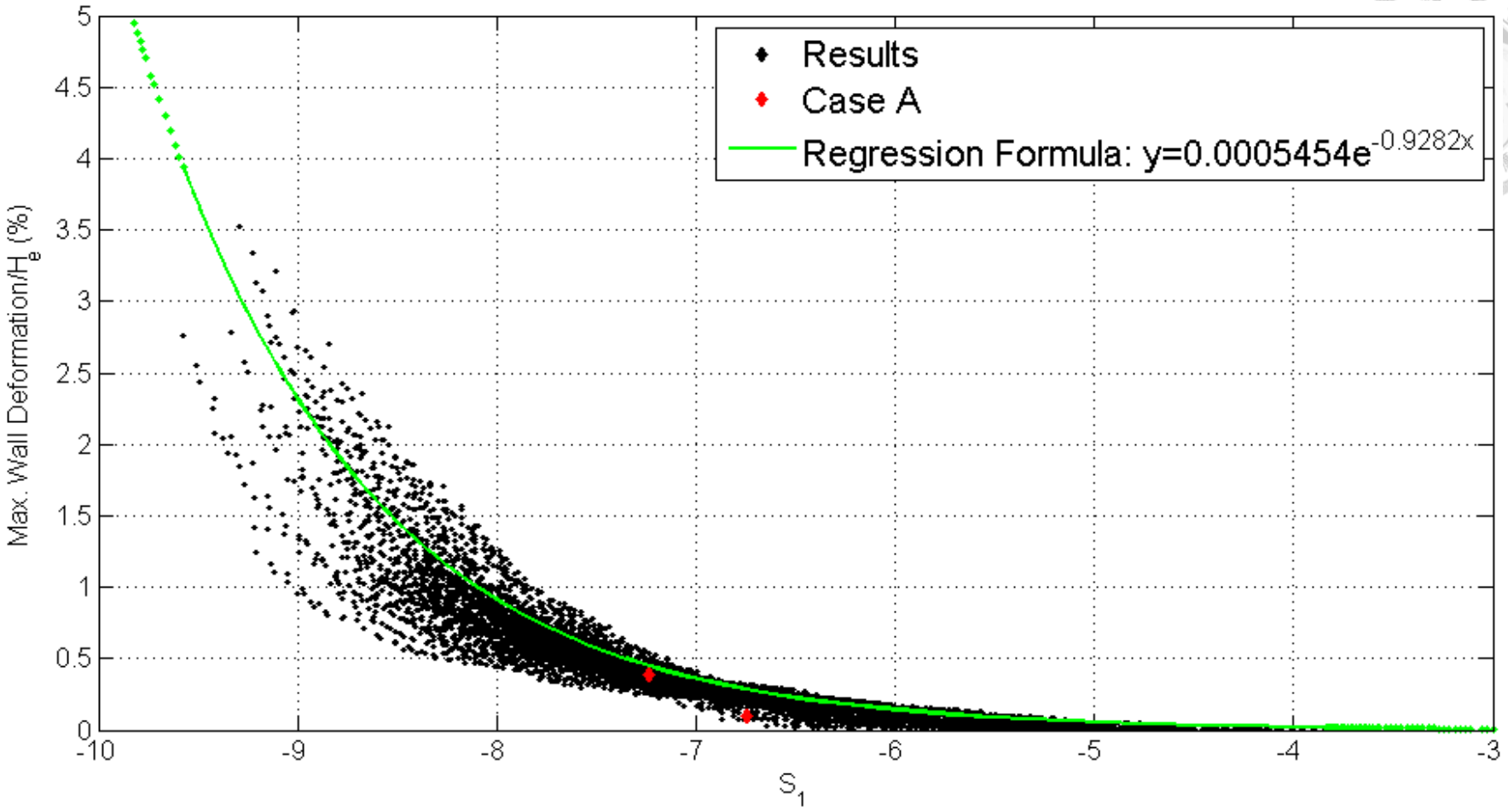

Fig.4. 7 New design charts with S_1 versus deformation.

doi:10.6342/NTU201600809

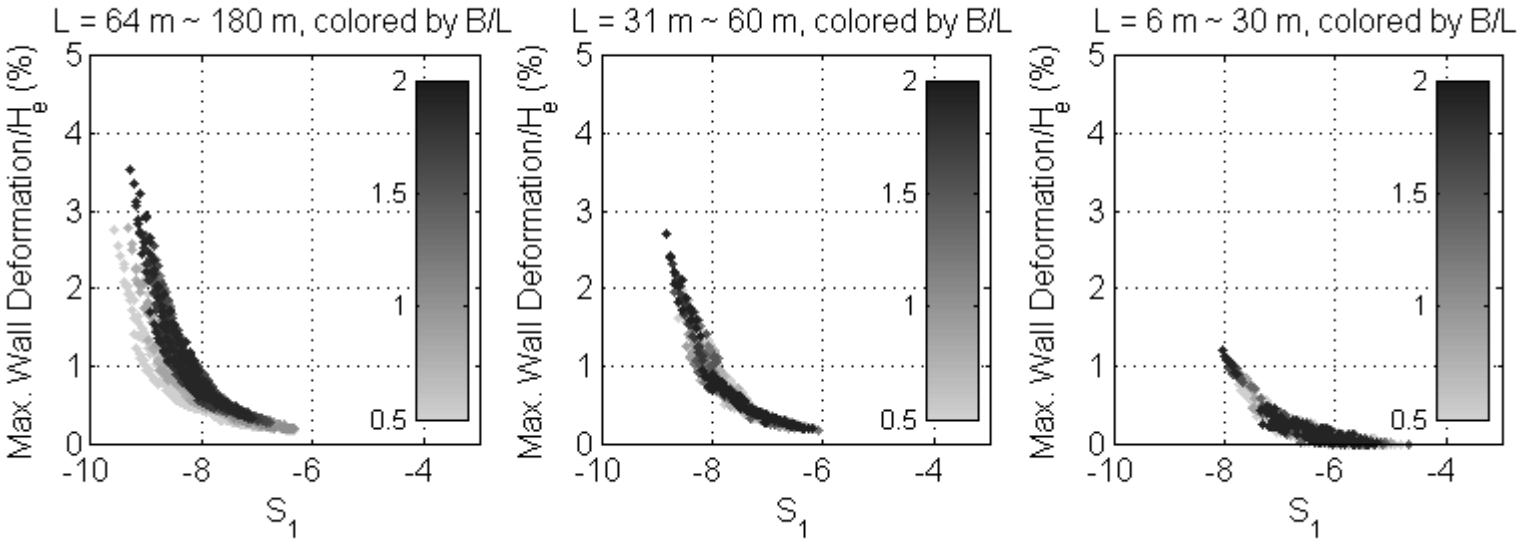

Fig.4. 8 Design charts of different range of L colored by B/L.

doi:10.6342/NTU201600809

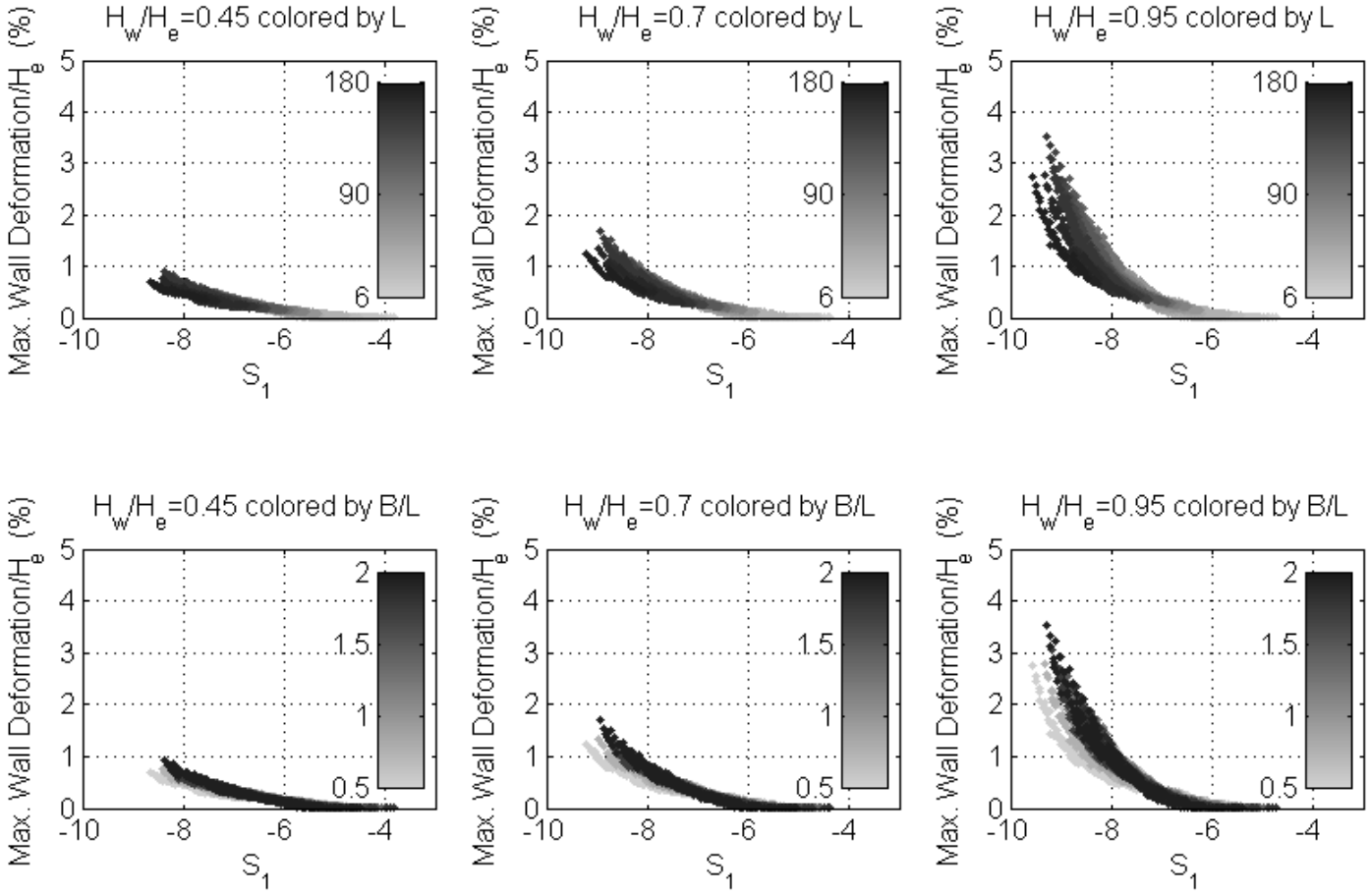

Fig.4. 9 Design charts of different H_w/H_e colored by L and B/L.

doi:10.6342/NTU201600809

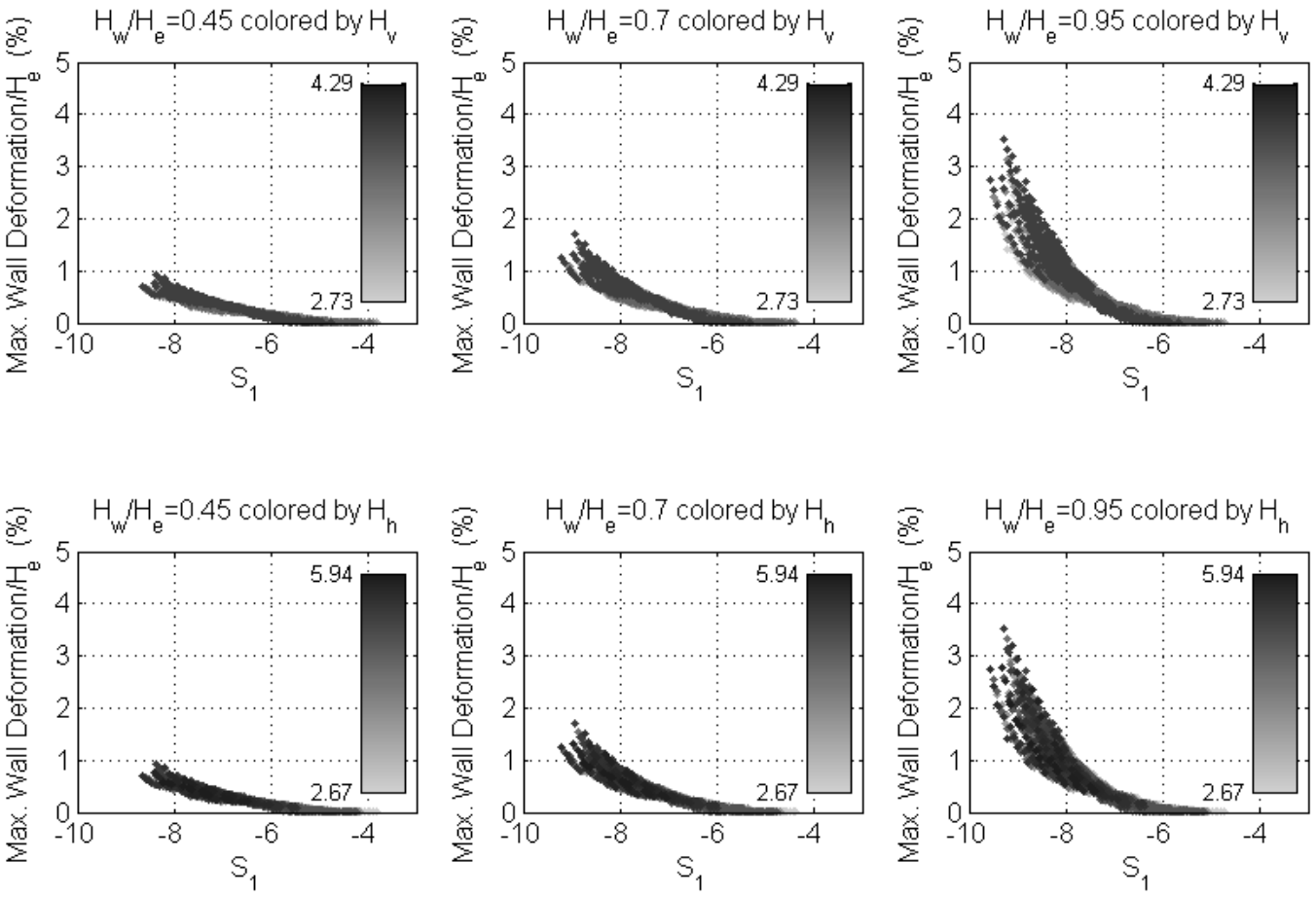

Fig.4. 10 Design charts of different H_w/H_e colored by H_v and H_h.

doi:10.6342/NTU201600809

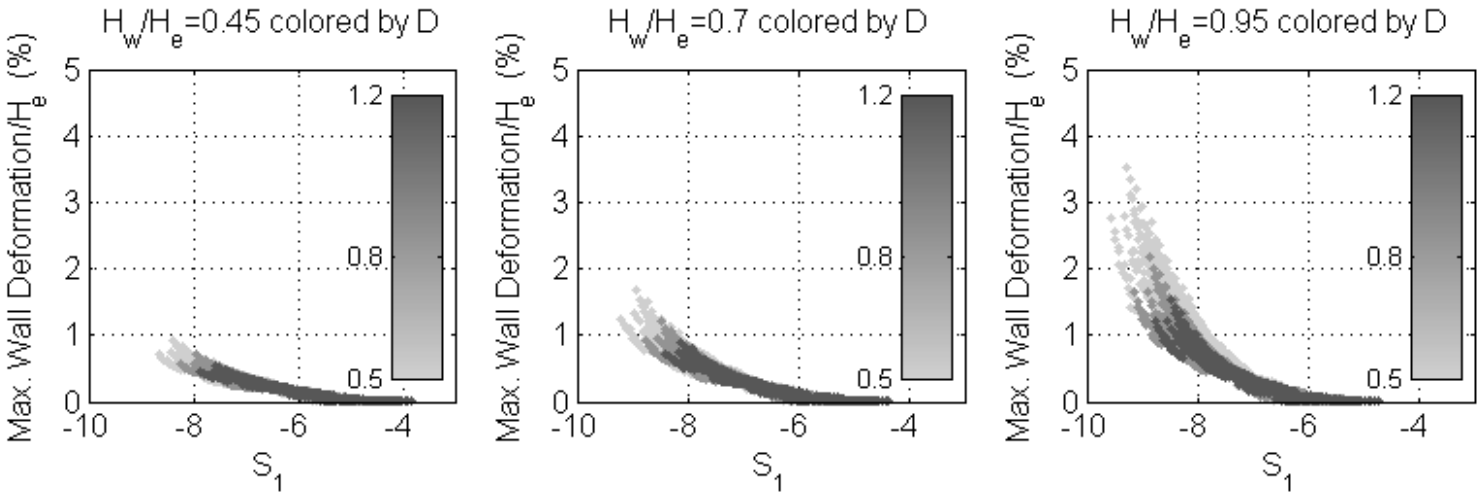

Fig.4. 11 Design charts of different H_w/H_e colored by D.

doi:10.6342/NTU201600809

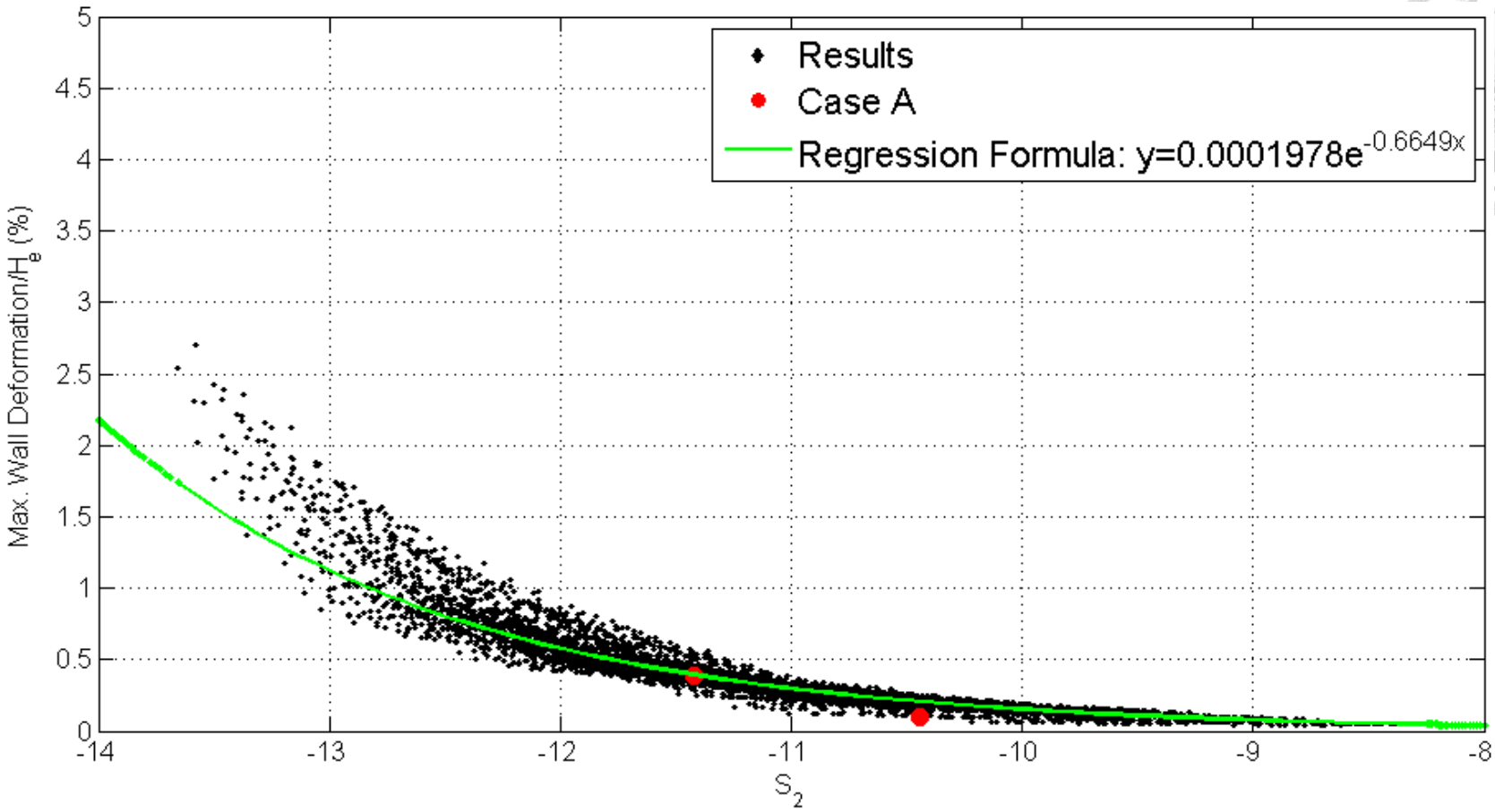

Fig.4. 12 New design charts with S_2 versus deformation.

doi:10.6342/NTU201600809

Table 4. 1 Parameters of soil, wall, and struts.

	Unit	Value
Soil		
γ	kN/m^3	20
E’	kN/m^2	50000
υ’	-	0.3
c’	kN/m^2	0
φ’	°	30
ψ	°	0
Wall		
γ (*)	kN/m^3	4
E’	kN/m^2	24630000
υ’	-	0.2
Struts		
EA	kN	2438000

*NOTE: According to manuals of PLAXIS, the plate element itself does not occupy any volume and overlaps with the soil elements. It might be considered to subtract the unit soil weight from the real unit weight of plate to compensate for the overlap. Hence, the unit weight of wall is very small in this table.

doi:10.6342/NTU201600809

Table 4. 2 Dimensions of excavations in Group A.

	L/H_e																	
	0.5			1.0			1.5			2.0			2.5			3.0		
L/B	L	B	B/H_e	L	B	B/H_e	L	B	B/H_e	L	B	B/H_e	L	B	B/H_e	L	B	B/H_e
0.5	10	20	1.00	20	40	2.00	30	60	3.00	40	80	4.00	50	100	5.00	60	120	6.00
0.7	10	14	0.71	20	29	1.43	30	43	2.14	40	57	2.86	50	71	3.57	60	86	4.29
1.1	10	9	0.45	20	18	0.91	30	27	1.36	40	36	1.82	50	45	2.27	60	55	2.73
1.3	10	8	0.38	20	15	0.77	30	23	1.15	40	31	1.54	50	38	1.92	60	46	2.31
1.7	10	6	0.29	20	12	0.59	30	18	0.88	40	24	1.18	50	29	1.47	60	35	1.76

doi:10.6342/NTU201600809

Table 4. 3 Dimensions of excavations in Group B.

	L/H_e																	
	0.5			1.0			1.5			2.0			2.5			3.0		
L/B	L	B	B/H_e	L	B	B/H_e	L	B	B/H_e	L	B	B/H_e	L	B	B/H_e	L	B	B/H_e
0.5	15	30	1.00	30	60	2.00	45	90	3.00	60	120	4.00	75	150	5.00	90	180	6.00
0.7	15	21	0.71	30	43	1.43	45	64	2.14	60	86	2.86	75	107	3.57	90	129	4.29
1.1	15	14	0.45	30	27	0.91	45	41	1.36	60	55	1.82	75	68	2.27	90	82	2.73
1.3	15	12	0.38	30	23	0.77	45	35	1.15	60	46	1.54	75	58	1.92	90	69	2.31
1.7	15	9	0.29	30	18	0.59	45	26	0.88	60	35	1.18	75	44	1.47	90	53	1.76

doi:10.6342/NTU201600809

Chapter 5 Conclusions and Recommendations

From the work carried out in this study, several conclusions and recommendations can be drawn herein.

5.1 Conclusions

1. Wall deformations in large excavations.

   As can be seen in Fig.4.3, the stripe got wider while L increased, especially for L ranging from 64 m to 180 m. It was found that $\frac{B}{L}$ attributed the width of stripe in large L most, seen in Fig.4.8.

   As mentioned in chapter 4, the influence of $\frac{B}{L}$ is not clear. The distribution of different $\frac{B}{L}$ would change with the increment of L.

2. The influence of maximum water head differences on wall deformation.

   The maximum water head difference is the only factor which is not one of the geometry configurations. However, as can be seen in Fig.4.3 to Fig.4.6, it has greatest influence on wall deformation.

   However, $\frac{H_w}{H_e}$ only affected how long the exponential tendency developed, but it had no interactions with other factors.

3. Performance of new system stiffness.

   The new system stiffness, S_1 and S_2, worked much better on the long side than short side. We thought that it is because the influence of B is not clear in those form of system stiffness, as mentioned previously. On the long side of excavation, which had lower B, the wall deformation were affected by B less than short side. That is one of the deficiencies of new system stiffness.

doi:10.6342/NTU201600809

5.2 Recommendations

In this study, four factors, including $\frac{H_w}{H_e}$, soil profile, struts types and prestress, were not considered. $\frac{H_w}{H_e}$ was fixed as 2.0 in this study. For the future work, it can be examined with various diaphragm wall thickness D. The soil profile is also important. The soil profile in this study was limited to sandy soil. To make a design chart more extensively used, clayey soil should be taken into considerations, and multi-layered stratum could be simplified as average sandy and clayey soil parameters.

In practice, the strut pre-stress is usually applied about 50% of the allowable axial strength of struts, except on the first level of supports. The variations of struts types and pre-stress could be involved to make estimation of design chart more precise, but it might cause the chart too complicated to use.

The factors should be normalized before figuring out the power terms of them to obtain a dimensionless system stiffness for more general application.

Advanced soil constitutive models, capable of mimicking the nonlinear stress-strain behavior, shear dilatancy, loading-unloading hysteresis etc., can be used to simulate the behavior of excavation more precisely. Lastly, the influence of B on diaphragm wall deformation should be further examined.

doi:10.6342/NTU201600809

REFERENCE

[1] Bowles, J. E., (1996). "Foundation Analysis and Design". 5th Edition, McGraw-Hill Book Company, New York, USA.

[2] Bryson, L. S., and Zapata-Medina, D. G. (2012). "Method of Estimation System Stiffness for Excavation Support Walls". *Journal of Geotechnical and Geoenvironmental Engineering*, Vol. 138, 1104-1115.

[3] Chua, H. Y., and Bolton, M. D. (2005). "Modeling of Horizontal Arching on Retaining Walls". *International Conference on Soil Mechanics and Geotechnical Engineering*, Vol. 3, 1455-1459.

[4] Dao, S. D. (2015). "Application of Numerical Analysis for Deep Excavations in Soft Ground". Taiwan, National Kaohsiung University of Applied Sciences.

[5] Finno, R. J., Blackburn, J. T., and Roboski, J. F. (2007). "Three-Dimensional Effects for Supported Excavations in Clay". *Journal of Geotechnical and Geoenvironmental Engineering*, Vol. 133, 30-36.

[6] Finno, R. J., Bryson, L. S., and Calvello, M. (2002). "Performance of a Stiff Support System in Soft Clay". *Journal of Geotechnical and Geoenvironmental Engineering*, Vol. 128, 660-671.

[7] Finno, R. J., Calvello, M. (2005). "Supported Excavations: Observational Method and Inverse Modeling". *Journal of Geotechnical and Geoenvironmental Engineering*, Vol. 131, 826-836.

[8] Hsieh, H. S., Cherng, J. C., and Huang, H. F. (2010). "A Note on the Diaphragm Wall Design for Small/Medium Size Excavations". *Sino-Geotechnics*, No.123, 15-22.

doi:10.6342/NTU201600809

[9] Hsiung, B. B. C. (2009), “A Case Study on the Behavior of a Deep Excavation in Sand”. *Computers and Geotechnics*, Vol. 36, 665-675.

[10] Khoiri, M., and Ou, C. Y. (2013). “Evaluation of Deformation Parameter for Deep Excavation in Sand through Case Studies”. *Computers and Geotechnics*, Vol. 47, 57-67.

[11] Lee, F. H., Yong, K. Y., Quan C. N., and Chee, K. T. (1998). “Effect of Corners in Strutted Excavations: Field Monitoring and Case Histories”. *Journal of Geotechnical and Geoenvironmental Engineering*, Vol. 124, 339-349.

[12] Likitlersuang, S., Surarak, C., Wanatowski, D., Oh, E., and Balasubramaniam, A. (2013). “Finite Element Analysis of a Deep Excavation: A Case Study from the Bangkok MRT”, *Soil and Foundations*, Vol. 53, No. 5, 756-773.

[13] Lim, A., Ou, C. Y., and Hsieh, P. G. (2010). “Evaluation of Clay Constitutive Models for Analysis of Deep Excavation under Undrained Conditions”. *Journal of GeoEngineering*, TGS, Vol. 5, No. 1, 9-20.

[14] Marr, W., and Hawkes, M. (2010). “Displacement-Based Design for Deep Excavations”. *Earth Retention Conference*, Vol.3, pp. 82-100.

[15] Meng, L. J., Zhang, Y. J., and Ma, X. W. (2015). “A Numerical Analysis Method for Active Earth Pressure behind a Retaining Wall Considering Soil Arching Effect”. *Electronic Journal of Geotechnical Engineering*, Vol. 20, Bund. 8.

[16] Ou, C. Y. (2016). “Finite Element Analysis of Deep Excavation Problems”. *Journal of GeoEngineering*, Vol. 11, No. 1.

[17] Ou, C. Y., Chiou, D. C., and Wu, T. S. (1996). "Three-Dimensional Finite Element Analysis of Deep Excavations." *Journal of Geotechnical Engineering*, 122:5, 337-345.

[18] Wu, C. H., Ou, C. Y. and Tung, N. (2010). “Corner Effects in Deep

doi:10.6342/NTU201600809

Excavations-Establishment of a Forecast Model for Taipei Basin T2 Zone". *Journal of Marin Science and Technology*, Vol. 18, No. 1, 1-11.

doi:10.6342/NTU201600809